

Quasi-two-dimensional organic superconductors: a review .

John Singleton^{1,2} and Charles Mielke.

¹National High Magnetic Field Laboratory, Los Alamos National Laboratory,
MS-E536, Los Alamos, New Mexico 87545, USA

²University of Oxford, Department of Physics, The Clarendon Laboratory, Parks
Road, Oxford OX1 3PU, U.K.

Abstract. We present a review of quasi-two-dimensional organic superconductors. These systems exhibit many interesting phenomena, including reduced dimensionality, strong electron-electron and electron-phonon interactions and the proximity of antiferromagnetism, insulator states and superconductivity. Moreover, it has been possible to measure the electronic bands of many of the organics in great detail, in contrast to the situation in other well-known systems in which similar phenomena occur. We describe the crystal structure and normal-state properties of the organics, before presenting the experimental evidence for and against exotic superconductivity mediated by antiferromagnetic fluctuations. Finally, three instances of field-induced unconventional superconductivity will be described.

1. Introduction

Over the past fifteen years there has been an increasing scientific interest in crystalline organic metals and superconductors. These materials are made up of relatively small organic molecules constructed from carbon, sulphur, selenium, hydrogen and the like, combined with a second molecular species, either inorganic or organic. One usually thinks of solids made up from organic molecules as insulators; however, the crystalline organic metals conduct electricity, and their low temperature resistivity usually decreases with decreasing temperature, a classic signature of more conventional (elemental) metals.

The reason for the current intense interest in organic metals is that they form a uniquely flexible system for the study of superconductivity, magnetism and many-body effects [1, 2, 3, 4, 5]. In this context, the term "many-body effects" refers to the interactions experienced by the mobile electrons within the organic metal; in such systems, the electrons can no longer be thought of as independent entities, but instead interact with each other and with excitations such as phonons (i.e. the vibrations of the crystal lattice). Materials in which such many-body effects are important are often referred to as correlated electron systems.

Of course there are other interesting correlated-electron systems. Prime examples are the so-called "High T_c " cuprate superconductors (e.g. $\text{YBa}_2\text{Cu}_3\text{O}_{7-x}$) which have been the subject of considerable experimental and theoretical effort. Organic metals share many features with the cuprates (a quasi-two-dimensional bandstructure, the proximity of antiferromagnetism, superconductivity and insulating behaviour, unconventional superconductivity [1, 2, 3, 4, 5]) and yet they are much cleaner systems; it has been possible to measure many details of the electronic energy levels of the organics using accurate techniques [1, 6], whereas this has proved impossible in the cuprates. Finally, the organics are interesting because a variety of exotic phases have been predicted and measured at potentially accessible magnetic fields ($B \leq 50-100$ T) and temperatures [7, 8, 9].

The description "organic superconductor" can encompass quite a range of materials (e.g. quasi-one-dimensional superconductors of the form $(\text{TM T SF})_2\text{X}$ [10], derivatives of buckminsterfullerene [13] and the recently-discovered field-effect devices based on acene and its relatives [11]). Each of these is worth a review article in its own right. To avoid information overload, we shall therefore concentrate solely on the quasi-two-dimensional organic superconductors, which form a rich and diverse family of materials [1, 13]. These systems are also of interest because they are perhaps the closest organic relative of the above-mentioned cuprate superconductors [2, 3].

The review will describe the normal state properties of the organics, followed by a discussion of the proposed mechanisms for superconductivity. Afterwards, the superconducting phase diagram will be reviewed. Finally, we shall mention some recent instances of (in some cases exotic) field-induced superconductivity.

2. Normal-state properties

2.1. Crystal structure.

The electronic bands of quasi-two-dimensional organic superconductors are derived from molecular orbitals [12, 13]. A number of molecular species are used as band structure building blocks; bis(ethylenedithio)tetrathiofulvalene (also known as BEDT-TTF or ET; Figure 1) is a typical example [12, 13, 14].

Although such molecules look complicated (and their acronym may seem daunting) at first sight, the principles behind their use in the construction of crystalline organic metals are very simple. For example, the BEDT-TTF molecule is roughly flat, so that it can be packed in a variety of arrangements in a solid, and it is surrounded by voluminous molecular orbitals; to create electronic bands, it is merely necessary to stack the BEDT-TTF molecules next to each other, so that the molecular orbitals can overlap. Crudely one might say that this enables the electrons to transfer from molecule to molecule.

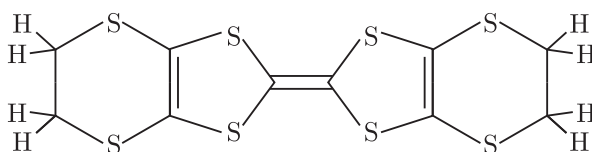


Figure 1. The bis(ethylenedithio)tetrathiofulvalene (BEDT-TTF) molecule.

Most of the molecules used to create quasi-two-dimensional organic superconductors are of a similar form to BEDT-TTF; for example, when the innermost four sulphur atoms of BEDT-TTF are replaced by selenium, one obtains BETS (bis(ethylenedithio)tetraseleenafulvalene) [12], which can also be used to produce organic superconductors. Other varieties include BEDO [12, 15] and MDT-TTF [12].

Returning to our initial example, in order to form the band structure, BEDT-TTF molecules must be stacked next to each other so that the molecular orbitals overlap. This arrangement of the band structure-forming molecules in an ordered arrangement is usually accomplished by making a charge-transfer salt [1, 12, 13, 14]. In a charge-transfer salt, a number j of BEDT-TTF molecules will jointly donate an electron to a second type of molecule (or collection of molecules) which we label X , to form the compound $(\text{BEDT-TTF})_jX$; owing to its negative charge, X is known as the anion, while the BEDT-TTF molecule is sometimes referred to as the donor or cation. The transfer of charge serves to bind the charge-transfer salt together (in a manner analogous to ionic bonding) and also leaves behind a hole, jointly shared between the j BEDT-TTF molecules. This means that the bands formed by the overlap of the BEDT-TTF

^z The term band refers to the distribution of mobile electronic states within a solid. As we shall see below, bands are characterised by dispersion relationships, formulae which relate the energies $E(k)$ of the mobile electronic states to their wavevector quantum numbers k . For a summary, see e.g. Chapters 2-4 of Reference [16].

^x A hole is an empty electronic state in an electronic band. As far as electrical conduction is concerned, the properties of a hole are formally equivalent to those of a positively charged particle with the same

molecular orbitals will be partially filled, leading one to expect that the charge-transfer salt will conduct electricity.

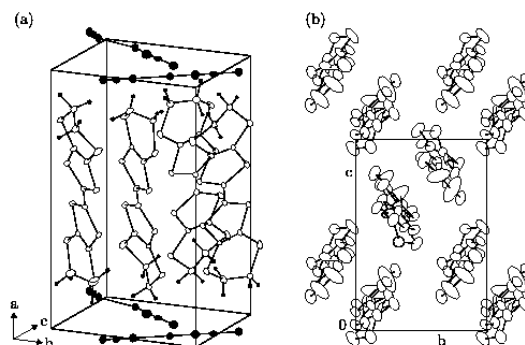


Figure 2. Structure of the BEDT-TTF charge-transfer salt $-(\text{BEDT-TTF})_2\text{Cu}(\text{NCS})_2$ ($T_c = 10.4 \text{ K}$ superconductor). (a) Side view of molecular arrangement; the BEDT-TTF molecules pack in planes separated by layers of the smaller $\text{Cu}(\text{NCS})_2$ anions. (b) View downwards onto the BEDT-TTF planes, showing that the BEDT-TTF molecules are packed closely together, allowing substantial overlap of the molecular orbitals. The unit cell edges are 16.248 \AA , 8.44 \AA and 13.124 \AA at room temperature. (After Reference [17].)

Figure 2 [17] shows the molecular arrangements in the BEDT-TTF charge-transfer salt $-(\text{BEDT-TTF})_2\text{Cu}(\text{NCS})_2$, a $T_c = 10.4 \text{ K}$ superconductor. (Here the c denotes the packing arrangement of the BEDT-TTF molecules; often several different packing arrangements can be achieved with one particular anion.) The BEDT-TTF molecules are packed into layers, separated by layers of the $\text{Cu}(\text{NCS})_2$ anion molecules. Within the BEDT-TTF layers, the molecules are in close proximity to each other, allowing substantial overlap of the molecular orbitals; the transfer integrals [16], which parameterise the ease of hopping of electrons between BEDT-TTF molecules, will be relatively large within the BEDT-TTF planes. Conversely, in the direction perpendicular to the BEDT-TTF planes, the BEDT-TTF molecules are well separated from each other; the transfer integrals will be much smaller in this direction (i.e. hopping is more difficult). This extreme anisotropy, resulting from a layered structure, is typical of most quasi-two-dimensional organic superconductors; it results in electronic properties which for many purposes can be considered to be two dimensional. We shall return to the question of dimensionality below.

Figure 3 shows another BEDT-TTF charge-transfer salt, $-(\text{BEDT-TTF})_2\text{I}_3$ (again c denotes the packing arrangement of the BEDT-TTF molecules) [18]. As in the case of $-(\text{BEDT-TTF})_2\text{Cu}(\text{NCS})_2$ (Figure 2), the BEDT-TTF molecules pack in planes separated by layers of the smaller anions, in this case I_3 molecules. However, the packing arrangement of the BEDT-TTF molecules is considerably different from that in $-(\text{BEDT-TTF})_2\text{Cu}(\text{NCS})_2$.

velocity as that of the (empty) electronic state. For a simple introduction to the concept of holes, see e.g. Reference [16], Chapter 5.

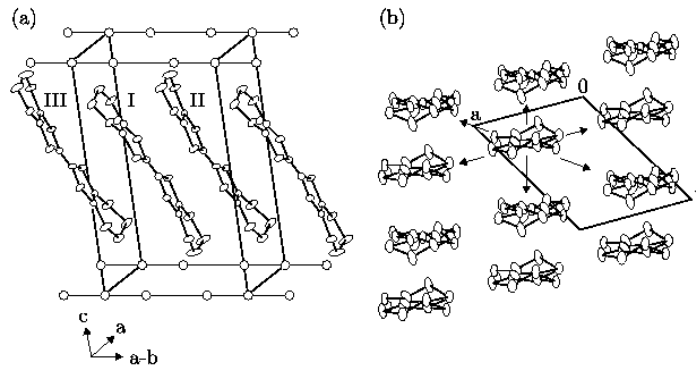


Figure 3. Structure of the BEDT-TTF charge-transfer salt $-(\text{BEDT-TTF})_2\text{I}_3$. (a) Side view of molecular arrangement. As in Figure 2, the BEDT-TTF molecules pack in planes separated by layers of the smaller anions; in this case the anions are I_3^- molecules. (b) View downwards onto the BEDT-TTF planes, showing that the BEDT-TTF molecules are packed closely together, allowing substantial overlap of the molecular orbitals [18]. However, the packing arrangement of the BEDT-TTF molecules is considerably different from that in $-(\text{BEDT-TTF})_2\text{Cu}(\text{NCS})_2$ (see Figure 2).

A comparison of Figures 2 and 3 shows that charge-transfer salts are an extremely flexible system with which to study the physics of band formation; by changing the anion, one can make the BEDT-TTF molecules pack in different arrangements. As the BEDT-TTF molecules are long and flat (unlike single atoms), the transfer integrals will depend strongly on the way in which the BEDT-TTF molecules are arranged with respect to each other; this will be reflected in the shape of the resulting bands [12, 13]. It is therefore convenient to classify charge-transfer salts according to their crystal structures, as each packing arrangement results in a distinct electronic-band topology. The main arrangements are labelled the α , β , γ , δ , ϵ , ζ , and η phases [12].

More subtle changes are possible within a particular morphology. It is possible to make α -phase salts of the form $-(\text{BEDT-TTF})_2\text{X}$ using several different anion molecules X, for example I_3^- , IBr_2^- , AuI_2^- etc.. The different possible anions have slightly different lengths; therefore the size of the unit cell can be varied by using different anions (see Figure 3). Figure 4 shows the relationship between superconducting critical temperature T_c and hydrostatic pressure for three α -phase salts. It can be seen that increasing the pressure (which decreases the unit cell size) lowers T_c ; substitution of a larger anion increases the unit cell size, countering the effect.

The use of different anions to vary the unit cell size is often referred to as "chemical pressure". We shall return to the variation of T_c with pressure in Sections 2.5 and 3.1.1.

2.2. Intralayer Fermi surface topologies

The defining property of a metal is that it possesses a Fermi surface, that is, a constant-energy surface in k -space which separates the filled electron states from empty electron

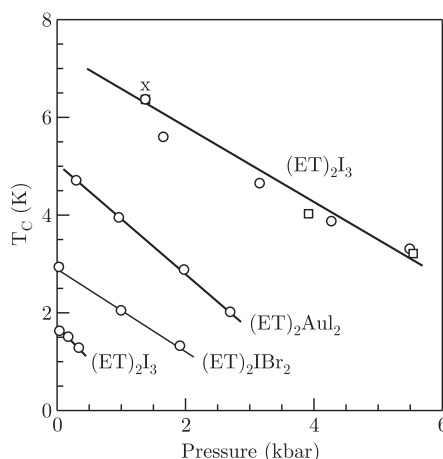


Figure 4. Superconducting critical temperature T_c versus hydrostatic pressure for three phase BEDT-TTF (ET) salts. Decreasing the unit cell size, either by using a shorter anion or by increasing the pressure, reduces T_c [19]. (Note that $-(BEDT-TTF)_2I_3$ undergoes a structural phase transition at about 0.6 kbar.)

states at absolute zero ($T = 0$). The energy of a quasiparticle at the Fermi surface is known as the Fermi energy, E_F . The shape of the Fermi surface is determined by the dispersion relationships (energy versus k relationships) $E = E(k)$ of each partially-filled band and the number of electrons (or holes) to be accommodated. Virtually all of the properties of a metal are determined by the quasiparticles at the Fermi surface, as they occupy states which are adjacent in energy to empty states; therefore they are able to respond to external forces and other perturbations (see e.g. Chapters 1, 2 and 8 of Reference [16]).

As has been mentioned in the preceding section, the organic superconductors discussed in this review are highly anisotropic; most of the quasiparticle motion occurs within the highly-conducting planes. The Fermi-surface topology is dominated by this consideration; the interlayer motion is far less important. In this section we shall therefore examine the cross-sections of the Fermi surfaces parallel the highly-conducting planes; the slight variations in Fermi-surface cross-sectional area will be discussed in Section 2.3.

2.2.1. General description Figure 5(a) shows a section (parallel to the highly-conducting planes) through the first Brillouin zone and Fermi surface of $-(BEDT-TTF)_2Cu(NCS)_2$ [5, 20, 21]. The Fermi surface may be understood by examining Figure 2(b) [23]. Note that the BEDT-TTF molecules are packed in pairs called dimers; if we consider each dimer as a unit, it will be seen that it is surrounded by four other dimers. We thus expect the bandstructure to be fairly isotropic in the plane, because

The term quasiparticle refers generally to a conduction electron or hole modified by the effects of electron-electron and electron-phonon interactions [24]. We shall discuss this in more detail in Section 2.4; until then, the reader is advised to regard quasiparticle as a general term for an electron or hole in a solid (see e.g. Reference [16], Chapter 8).

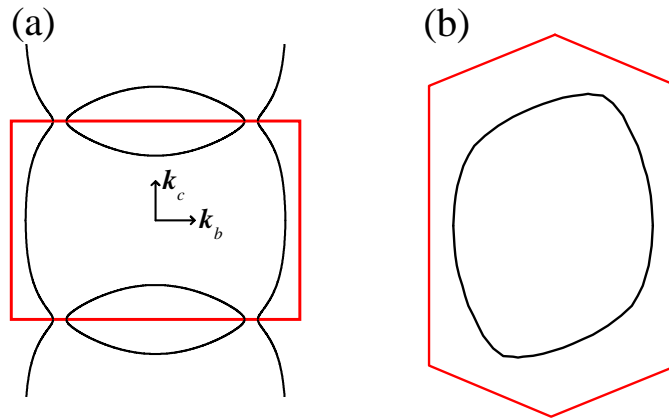


Figure 5. (a) Brillouin zone and Fermi surface of $-(\text{BEDT-TTF})_2\text{Cu}(\text{NCS})_2$, showing the open, quasi-one-dimensional sections, and the closed, quasi-two-dimensional pocket [5, 20, 21]. (b) Brillouin zone and Fermi surface of $-(\text{BEDT-TTF})_2\text{IBr}_2$ [22].

there will be substantial, similar transfer integrals in these four directions. The unit cell contains two dimers, each of which contributes a hole (in the charge-transfer process, two BEDT-TTF molecules jointly donate one electron to the anion). Thus, to a first approximation, the Fermi surface for holes might be expected to be roughly circular with the same area as the Brillouin zone (as there are two holes per unit cell). As can be seen from Figure 5(a), the Fermi surface is roughly like this; however, the Fermi surface intersects the Brillouin zone boundaries in the c direction, so that band gaps open up (see e.g. Chapter 2 of Reference [16]). The Fermi surface thus splits into open (electron-like) sections (often known as Fermi sheets) running down two of the Brillouin-zone edges and a closed hole pocket (referred to as the "pocket") straddling the other; it is customary to label such sections "quasi-one-dimensional" and "quasi-two-dimensional" respectively. The names arise because the group velocity v of the electrons is given by [16, 24][†]

$$\hbar v = \nabla_{\mathbf{k}} E(\mathbf{k}): \quad (1)$$

The Fermi surface is a surface of constant energy; Equation 1 shows that the velocities of electrons at the Fermi surface will be directed perpendicular to it. Therefore, referring to Figure 5, electrons on the closed Fermi-surface pocket can possess velocities which point in any direction in the (k_b, k_c) plane; they have freedom of movement in two dimensions and are said to be quasi-two-dimensional. By contrast, electrons on the open sections have velocities predominantly directed parallel to k_b and are quasi-one-dimensional.

{ The Brillouin-zone is the primitive unit cell of the reciprocal (k -space) lattice. The k -space size of the Fermi surface follows from the properties of phase-space. Each quasiparticle donated by a unit cell contributes a volume to the Fermi surface equivalent to half the volume of the Brillouin zone. See e.g. Reference [16], Chapters 1, 2, 8 and Appendix A, or Reference [24].

[†] This equation is the three-dimensional analogue of the well-known formula for the group velocity of a wave packet propagating in one dimension, $v = (d\omega/dk)$.

β -phase BEDT-TTF superconductors $-(\text{BEDT-TTF})_2\text{X}$ can be made with a variety of other anion molecules, including $\text{X} = \text{Cu}[\text{N}(\text{CN})_2]\text{Br}$ (11.8 K), $\text{Cu}[\text{N}(\text{CN})_2]\text{Cl}$ (12.8 K (under pressure)), and I_3 (4 K); here the number in parentheses represents T_c . In all of these salts, the Fermi-surface topology is very similar to that in Figure 5(a); small differences in the symmetry of the anion layer lead to variations in the gap between the quasi-one-dimensional and quasi-two-dimensional Fermi-surface sections [1, 12, 13]. A summary of the detailed differences and effective masses is given in Section 3.2 of Reference [1] (see also [12]).

Figure 5(b) shows the Fermi-surface topology and Brillouin zone of $-(\text{BEDT-TTF})_2\text{IBr}_2$ [22]. In this case (see Figure 3) there is one hole per unit cell, so that the Fermi surface cross-sectional area is half that of the Brillouin zone; only a quasi-two-dimensional pocket is present.

We have therefore seen that the bandstructure of a charge-transfer salt is chiefly determined by the packing arrangement of the cation molecules. As sources of superconductors, the α , β , γ , and δ phases have been the most important. The latter four phases all have predicted Fermi surfaces consisting of a quasi-two-dimensional pocket plus a pair of quasi-one-dimensional Fermi sheets (the pocket arrangement differs from phase to phase) [1, 6, 12]; the β -phase is alone in possessing a Fermi surface consisting of a single quasi-two-dimensional pocket [13].

2.2.2. Bandstructure calculations The bandstructures of organic superconductors have usually been calculated using the extended Hückel (tight-binding) approach, which employs the highest occupied molecular orbitals (HOMOs) of the cation molecule [12]. Section 5.1.3 of Reference [13] discusses this approach and cites some of the most relevant papers. Whilst this method is usually quite successful in predicting the main features of the Fermi surface (e.g. the fact that there are quasi-one-dimensional and quasi-two-dimensional Fermi-surface sections), the details of the Fermi-surface topology are sometimes inadequately described (see e.g. [25]). This can be important when, for example, the detailed corrugations of a Fermi sheet govern the interactions which determine its low-temperature groundstate [5, 25]. A possible way around this difficulty is to make slight adjustments of the transfer integrals so that the predicted Fermi surface is in good agreement with experimental measurements [5, 20, 21, 25]. In the γ and δ phases the predicted bandstructure seems very sensitive to the choice of basis set, and the disagreement between calculation and measurement is often most severe (see e.g. [26, 27, 28, 29]).

More sophisticated Hubbard-unrestricted Hartree-Fock band calculations have been carried out for $-(\text{BEDT-TTF})_2\text{Cu}(\text{NCS})_2$ [30]. These calculations attempt to take into account many-body effects, and are successful in reproducing a number of experimental

The effective mass parameterises the way in which a quasiparticle can respond to an external force. As we shall see below, the effective mass also gives a measure of the density of quasiparticle states at the Fermi energy. See e.g. Reference [24] or Reference [16], Chapter 5.

] Simple introductions to the tight-binding model of bandstructure are given in References [16, 24].

properties. They also indicate the importance of both antiferromagnetic fluctuations and electron-phonon interactions in $-(\text{BEDT-TTF})_2\text{Cu}(\text{NCS})_2$, a fact to which we shall return in Sections 3.1.1 and 3.4.

2.2.3. Experimental measurements of Fermi-surface topology. The low scattering rates in quasi-two-dimensional organic superconductors mean that it is possible to use a range of techniques to make accurate measurements of the Fermi-surface topology. The experimental techniques have been described in other reviews [1, 6, 13, 31, 32, 33]. We shall mention a few of the more important examples.

de Haas-van Alphen and Shubnikov-de Haas oscillations. In a magnetic field, the motion of quasiparticles becomes partially quantised according to the equation [16, 24]

$$E(\mathbf{B}; k_z; l) = \frac{\hbar e B}{m} \left(l + \frac{1}{2} \right) + E(k_z): \quad (2)$$

Here $E(k_z)$ is the energy of the (unmodified) motion parallel to \mathbf{B} , l is a quantum number (0; 1; 2; ...) and m is an orbitally-averaged effective mass. The magnetic field quantises the motion of the quasiparticles in the plane perpendicular to \mathbf{B} ; the resulting levels are known as Landau levels, and the phenomenon is called Landau quantisation. The Landau-level energy separation is given by \hbar multiplied by the angular frequency $\omega_c = \hbar e B / m$; this is known as the cyclotron frequency because it corresponds to the semiclassical frequency at which the quasiparticles orbit the Fermi surface [16, 24].

Magnetic quantum oscillations [1, 6, 34] are caused by the Landau levels passing through the Fermi energy. This results in an oscillation of the electronic properties of the system, periodic in $1/B$. From an experimental standpoint, the oscillations are usually measured in the magnetisation (de Haas-van Alphen effect) or the resistivity (Shubnikov-de Haas effect) [1, 6, 34].

Landau quantisation only occurs for sections of Fermi surface corresponding to semiclassical closed k -space orbits in the plane perpendicular to \mathbf{B} ; the frequency of the oscillation (in Tesla) is given by $F = (h/2e)A$, where A is the cross-sectional k -space area of the orbit [1, 6, 34]. An example is given in Figure 6, which shows Shubnikov-de Haas oscillations in the magnetoresistance of $-(\text{BEDT-TTF})_2\text{Cu}(\text{NCS})_2$ [35, 36] (the field was applied perpendicular to the quasi-two-dimensional planes). Turning first to Figure 6(a), a single frequency of oscillations is observed, caused by the quasi-two-dimensional pocket of the Fermi surface. The frequency (600 T in this case) allows one to deduce the cross-sectional area of the pocket [1, 6]. On increasing the temperature, the oscillations decrease in amplitude, owing to the thermal smearing of the Fermi-Dirac distribution function [1, 16]. The temperature dependence of the oscillation amplitude can be used to derive the orbitally-averaged effective mass of the quasiparticles orbiting the pocket [1, 6] ($3.5 \pm 0.1 m_e$ in this case [20, 35, 37]).

z Introductions to magnetic quantum oscillations, including the de Haas-van Alphen and Shubnikov-de Haas effects are given in Chapter 8 of Reference [16], or in Reference [24].

x Strictly it is the chemical potential μ , rather than the Fermi energy, which is important here. However $\mu \approx E_F$ at $T = 0$, and $\mu \approx E_F$ for virtually all experimental temperatures of interest [16, 24].

Finally, the oscillations increase in amplitude with increasing magnetic field; this field dependence allows one to derive the scattering time τ [1] (3 ps for the data shown [35]).

At higher magnetic fields (Figure 6(b)), an additional set of higher frequency oscillations becomes observable. These are due to a phenomenon known as magnetic breakdown; the cyclotron energy of the quasiparticles becomes high enough for them to tunnel (in k -space) across the gaps between the quasi-two-dimensional pocket and the quasi-one-dimensional sheets, so that a semiclassical orbit around the whole Fermi surface (a so-called γ orbit) can be completed [1, 38]. The large cross-sectional area of this orbit gives rise to a higher Shubnikov-de Haas oscillation frequency.

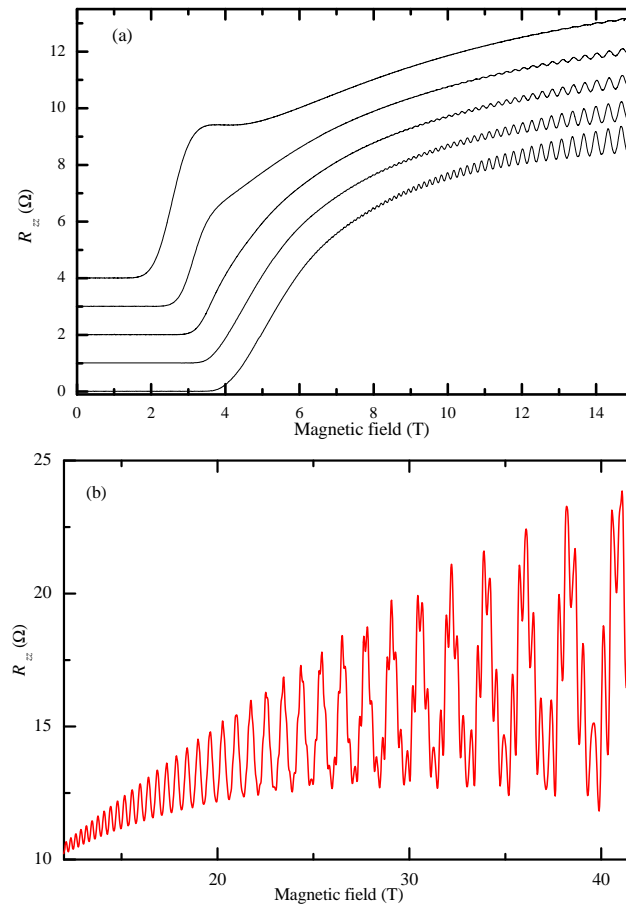


Figure 6. Magnetoresistance measurements of the organic superconductor – $(\text{BEDT-TTF})_2\text{Cu}(\text{NCS})_2$ (magnetic field applied perpendicular to the quasi-two-dimensional planes). (a) Low-field measurements, showing the superconducting to normal transition and, at higher fields, Shubnikov-de Haas oscillations caused by the quasi-two-dimensional pocket of the Fermi surface. Data for temperatures 1.96 K (uppermost trace), 1.34 K, 1.03 K, 800 mK and 620 mK (lowest trace) are shown; for clarity, the data have been offset by 1 [35]. (b) High-field experiment, showing higher frequency oscillations due to magnetic breakdown ($T = 480$ mK) [36]. In both cases, the current is applied in the interlayer direction, so that the measured R_{zz} is proportional to the interlayer resistivity component ρ_{zz} [1]. Similar data can be found in e.g. References [1, 37, 38].

Cyclotron resonance. Photons of frequency ω can be used to excite quasiparticles between Landau levels (see Equation 2) [1, 16]; the phenomenon is known as cyclotron resonance. The fundamental resonance occurs when $\hbar\omega_c = \hbar\omega$; for laboratory fields ($B \leq 20$ T) and the typical effective masses observed in organic superconductors [1], this corresponds to photon frequencies in the millimetre-wave range, $\omega \approx 10 - 100$ GHz. We shall discuss cyclotron resonance in more detail in Section 2.4.

Angle-dependent magnetoresistance oscillations and Fermi-surface-traversal resonances. Whilst they give very accurate information about the cross-sectional areas of the Fermi-surface sections, magnetic quantum oscillations do not provide any details of their shape. Such information is usually derived from angle-dependent magnetoresistance oscillations (AMROs) [1, 6, 32, 33]. AMROs are measured by rotating a sample in a fixed magnetic field whilst monitoring its resistance; the coordinate used to denote the position of AMROs is the polar angle θ between the normal to the sample's quasi-two-dimensional planes and the magnetic field [32, 33]. It is also very informative to vary the plane of rotation of the sample in the field; this is described by the azimuthal angle ϕ [32, 33].

AMROs result from the averaging effect that the semiclassical orbits on the Fermi surface have on the quasiparticle velocity. Both quasi-one-dimensional and quasi-two-dimensional Fermi-surface sections can give rise to AMROs; in the former case, the AMROs are sharp dips in the resistivity, periodic in \tan^{-1} ; in the latter case, one expects peaks, also periodic in \tan^{-1} [32, 33]. In order to distinguish between these two cases, it is necessary to carry out the experiment at several different ϕ . The ϕ -dependence of the AMROs can be related directly to the shape of a quasi-two-dimensional Fermi-surface section; in the case of a quasi-one-dimensional sheet, the AMROs yield precise information about the sheet's orientation [1, 6, 32, 33]. Typical data are shown in Figure 7.

Recently, a high-frequency variant of AMROs, known as the Fermi-surface-traversal resonance (FTR), has been developed. This technique allows additional information about the topology and corrugations of quasi-one-dimensional Fermi sheets to be deduced (see Reference [31] for a review).

2.3. 2D or not 2D? Measurements of the effective Fermi-surface dimensionality

We remarked in Sections 2.1 and 2.2.1 that the electronic properties of quasi-two-dimensional organic superconductors are very anisotropic. The band-structure-measuring techniques mentioned thus far chiefly give information about the intralayer topology of the Fermi surface. However, it is important to ask whether the Fermi surface is exactly two-dimensional, or whether it extends in the interlayer direction, i.e. is three-dimensional.

This question is of quite general interest, as there are many correlated-electron systems which have very anisotropic electronic bandstructure. In addition to the organic

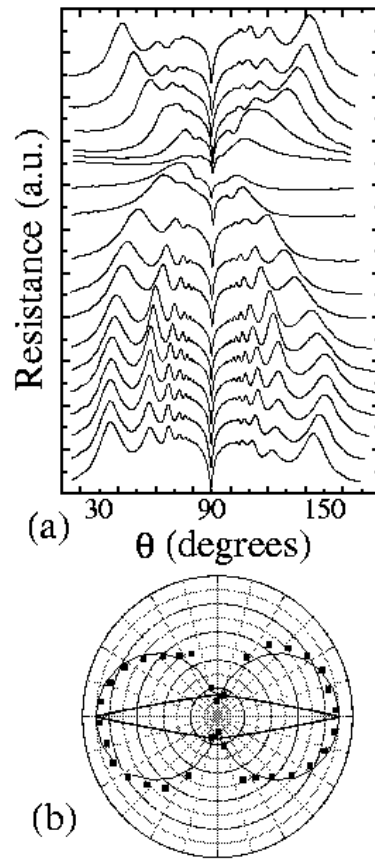


Figure 7. (a) AMRO data for ω -(BEDT-TTF) $_2$ SF $_5$ CH $_2$ CF $_2$ SO $_3$ at 10 T and 1.5 K for θ -angles 7.1 (top trace) 17.1, 27.1, ..., 177.1 (bottom trace—adjacent traces spaced by 10.1). $\theta = 0$ corresponds to rotation in the a^*c^* plane of the crystal to within the accuracy of the infrared orientation used. (b) The θ -dependence of the \tan^{-1} periodicity of the AMRO in (a) (points); the "figure of eight" solid curve is a fit. The resulting fitted FS pocket (elongated diamond shape) is shown within. The long axis of the pocket makes an angle of 68.4° with the b -axis. (After Reference [32].)

superconductors [1, 40], examples include the "high- T_c " cuprates [39, 40], and layered ruthenates [41] and manganites [42]. Such systems may be described by a tight-binding Hamiltonian in which the ratio of the interlayer transfer integral t_z to the average intralayer transfer integral t_{ij} is $\ll 1$ [1, 40, 43]. The inequality $\hbar\omega > t_z$ [44] where ω^{-1} is the quasiparticle scattering rate [39, 40, 43], frequently applies to such systems, suggesting that the quasiparticles scatter more frequently than they tunnel between layers. Similarly, under standard laboratory conditions, the inequality $k_B T > t_z$ often holds, hinting that thermal smearing will wipe out details of the interlayer periodicity [46].

The question has thus arisen as to whether the interlayer charge transfer is coherent or incoherent in these materials, i.e. whether or not the Fermi surface extends in the interlayer direction [1, 40, 43]. Incoherent interlayer transport is used as a justification

for a number of theories which are thought to be pivotal in the understanding of reduced-dimensionality materials (see e.g. [40, 46]). Moreover, models for unconventional superconductivity in π -phase BEDT-TTF salts invoke the nesting properties of the Fermi surface [4, 5, 47]; the degree of nesting might depend on whether the Fermi surface is a two-dimensional or three-dimensional entity (see [1], Section 3.5).

Many apparently solid experimental tests for coherence in organic superconductors have been deemed to be inconclusive [43]; e.g. semiclassical models can reproduce AMRO [32] and FTR data [31] equally well when the interlayer transport is coherent or "weakly coherent" [43].

A simple tight-binding expression is often used to simulate the interlayer (z -direction) dispersion [1]; $E(k_z) = 2t_z \cos(k_z a)$. Here t_z is the interlayer transfer integral and a is the unit-cell height in the z direction. The introduction of the interlayer dispersion causes a modulation of the Fermi-surface cross-section, shown schematically in Figure 8(a) [48, 49]. If the Fermi surface is extended in the z direction, a magnetic field applied exactly in the intralayer (xy) plane can cause a variety of orbits on the sides of the Fermi surface, as shown schematically in Figure 8(a). It has been proposed that the closed orbits about the belly of the Fermi surface [51] or the "self-crossing orbits" found under the same conditions [52] are very effective in averaging v_z , the interlayer component of the velocity. Therefore, the presence of such orbits will lead to an increase in the resistivity component ρ_{zz} [51, 52]. On tilting B away from the intralayer direction, the closed and "self-crossing" orbits cease to be possible when B has turned through an angle θ , where

$$(\text{in radians}) \quad \theta = \arctan(v_{ij}/v_z) \quad (3)$$

Here v_z is the maximum of the interlayer component of the quasiparticle velocity, and v_{ij} is the intralayer component of the quasiparticle velocity in the plane of rotation of B . Therefore, on tilting B around the in-plane orientation, one expects to see a peak in ρ_{zz} , of angular width 2θ , if (and only if [43]) the Fermi surface is extended in the z direction. By using Equations 1 and 3 and measured details of the intralayer Fermi-surface topology, it is possible to use ρ_{zz} to deduce t_z [21].

Figure 8(b) shows typical data for $-(\text{BEDT-TTF})_2\text{Cu}(\text{NCS})_2$. The observation of a peak in ρ_{zz} close to $\theta = 90^\circ$ allows the interlayer transfer integral to be estimated to be $t_z = 0.04$ meV [21]. This may be compared with intralayer transfer integrals

150 meV [20]. Such data are of great interest because they illustrate that the criteria used to delineate interlayer incoherence are rather a poor guide to real samples. For example, the sample shown in Figure 8(b) has $h = 6t_z$, and yet robustly shows evidence for a three-dimensional Fermi surface [21]. Similarly, a temperature of 5 K, ($k_B T = 10t_z$) leads one to expect incoherent interlayer transport [46], yet the peak in ρ_{zz}

k Nesting refers to a topological similarity between two sections of Fermi surface which allows one to be translated (by a so-called nesting vector) so that it exactly overlaps with the other. See e.g. References [13, 25].

{ The orbits are defined by the Lorentz force $\hbar(d\mathbf{k}/dt) = e\mathbf{v} \times \mathbf{B}$, where \mathbf{v} is given by Equation 1. This results in orbits on the Fermi surface, in a plane perpendicular to B [1, 24].

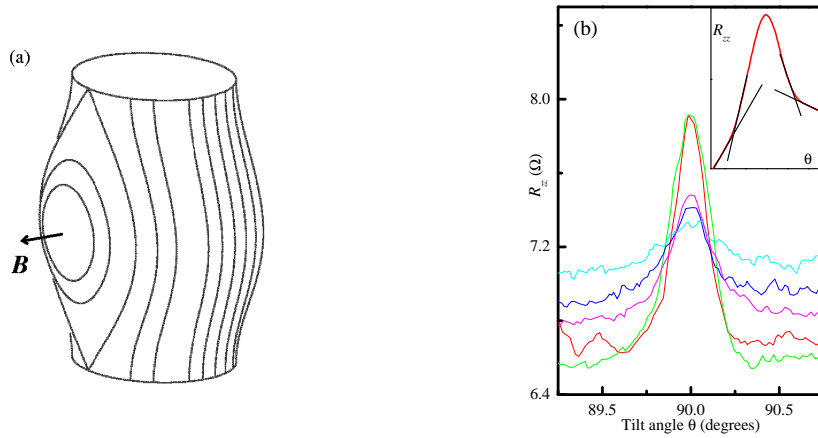


Figure 8. (a) Illustration of the effect of introducing interlayer dispersion on a quasi-two-dimensional Fermi surface section; the cross-section of the Fermi surface varies in the interlayer (k_z) direction. The lines on the sides of the Fermi surface illustrate some of the quasiparticle orbits caused by an in-plane field. (b) Interlayer resistance R_{zz} (proportional to ρ_{zz}) of a $-(\text{BEDT-TTF})_2\text{Cu}(\text{NCS})_2$ sample as a function of magnetic field orientation ($\theta = 90^\circ$ corresponds to magnetic field exactly in-plane). Data for temperatures $T = 0.48 \text{ K}, 1.4 \text{ K}, 3.0 \text{ K}, 4.4 \text{ K}$ and 5.1 K are shown. The background magnetoresistance increases with increasing T , whereas the peak at $\theta = 90^\circ$ becomes smaller. The inset shows the intersections of the linear extrapolations used to determine the peak width (after Reference [21]).

shown in Figure 8 (b) unambiguously demonstrates a three dimensional Fermi surface topology.

Such measurements have been carried out on the organic superconductors $-(\text{BEDT-TTF})_2\text{IBr}_2$ [22], $-(\text{BEDT-TTF})_2\text{Cu}_2(\text{CN})_3$ [54] (under pressure), $-(\text{BEDT-TTF})_2\text{NH}_4\text{Hg}(\text{SCN})_4$ [51] (under pressure), $-(\text{BEDT-TTF})_2\text{I}_3$ [51], $-(\text{BEDT-TTF})_2\text{Cu}(\text{NCS})_2$ [21], $-(\text{BETS})_2\text{GaCl}_4$ [29] and $^\infty-(\text{BEDT-TTF})_2\text{SF}_5\text{CH}_2\text{CF}_2\text{SO}_3$ [55, 56]. In the latter example, no peak was observed, suggesting incoherent interlayer transport. In all of the other instances, the ρ_{zz} data demonstrate a Fermi surface which is extended in the interlayer direction.

2.4. Renormalising interactions.

A simple bandstructure calculation essentially uses ions and molecules which are rigidly fixed in a perfectly periodic arrangement to obtain a periodic potential and hence the bands. However, the ions and/or molecules in a substance will in general be charged, or at the very least possess a dipole moment; as an electron passes through the solid, it will tend to distort the lattice around it owing to the Coulomb interactions between the ions and molecules and its own charge. This leads to the electron being accompanied

by a strain field as it moves through the substance; alternatively one can consider the electron being surrounded by virtual phonons, leading to a change in the electron's self energy [24]. Similarly, self-energy effects due to the interactions between the conduction electrons themselves must be taken into account [24, 57, 58].

The inclusion of such effects leads to the idea of "quasiparticles", excitations of an interacting electron system which obey Fermi-Dirac statistics and which "look like" conduction electrons or holes in many ways, but which possess renormalised effective masses and scattering rates [24, 58].⁺ In the presence of relatively weak interactions, it is possible to make predictions about the contribution to the quasiparticle effective mass caused by the above effects [57, 60]. If m_b is the band mass calculated in the bandstructure calculations, then the electron-lattice interactions discussed above will result in a dynamical mass, m^* , where

$$m^* = (1 + \lambda) m_b; \quad (4)$$

where λ is an electron-phonon coupling constant (in BEDT-TTF salts, λ is thought to be between 0.1 and 1 [59]). Finally, the electron-electron interactions result in an effective mass m^* ;

$$m^* = (1 + \frac{F_s^{-1}}{3}) m_b; \quad (5)$$

where F_s^{-1} is a constant known as a Fermi liquid parameter [57, 60].

How do such considerations affect experimental data? The interactions which give rise to the effective mass renormalisation chiefly affect states very close to the Fermi energy. Therefore, an interband optical measurement, which probes the full energy range of a band, is determined mostly by its bare (unrenormalised) width, enabling m_b to be extracted [20]. On the other hand, a cyclotron resonance experiment is expected to be relatively insensitive to interactions involving relative motion of electrons (i.e. the electron-electron interactions). The reason for this is that the wavelength of the photons used to excite cyclotron resonance (~ 1 mm) is much greater than the typical quasiparticle spacing (~ 10 Å), so that adjacent electrons experience an oscillatory electric field of the same phase; their relative separation is therefore not affected. Hence, the mass measured in cyclotron resonance will be close to the (orbitally averaged) dynamical mass, m^* [60]. Finally, the (orbitally averaged) effective mass (including the contributions of both electron-electron and electron-phonon interactions) is the mass measured in Shubnikov-de Haas and de Haas-van Alphen experiments [57, 60]. Following these ideas, Caulfield et al. compared optical spectra and Shubnikov-de Haas data in the superconductor $-(\text{BEDT-TTF})_2\text{Cu}(\text{NCS})_2$ [20], finding $m^* = m_b \approx 5$ [20, 61].

These considerations also motivated a number of attempts to observe cyclotron resonance in charge-transfer salts [57, 62]. For reasons discussed in Section 2.4.6

⁺ A collection of interacting electrons which can be treated (using Fermi-Dirac statistics) as a collection of quasiparticles is often known as a Fermi liquid; by contrast, a collection of non-interacting electrons is called a Fermi gas [24]. At present, it appears that most of the normal-state properties of quasi-two-dimensional organic superconductors are fairly well described by Fermi-liquid theory [1, 6, 13].

of Reference [1], many of the earlier experiments were seriously flawed, and reliable experiments had to await the development of resonant cavity techniques [63, 65, 64]. Since such measurements became feasible, only two superconducting salts have yielded cyclotron resonance data. In $-(\text{BEDT-TTF})_2\text{NH}_4\text{Hg}(\text{SCN})_4$, which is believed to have a simple Fermi surface consisting of a pair of sheets and a closed pocket, a cyclotron resonance corresponding to a mass of $1.9m_e$ was measured [64, 65]; this may be compared with an effective mass from magnetic quantum oscillations of $2.5m_e$ [67]. $^{10}-(\text{BEDT-TTF})_2\text{SF}_5\text{CH}_2\text{CF}_2\text{SO}_3$, again with a Fermi surface believed to consist of a single pocket and a pair of sheets (but see Reference [66]), exhibited a cyclotron resonance corresponding to a mass of $2.2m_e$ [31] (see Figure 9) the effective mass from Shubnikov-de Haas oscillations is $1.9m_e$ [68].

Thus it appears that the simple predictions of a large enhancement of the mass derived from magnetic quantum oscillations over that measured in a cyclotron resonance experiment do not hold. Recently, Kanki and Yamada [69] have carried out Hubbard-model calculations which contradict the simplistic theories [60, 70] and which appear to support the above experimental observations. Kanki and Yamada found that the relationship between the mass measured in a cyclotron resonance experiment and that derived from magnetic quantum oscillations depends strongly on e.g. band filling, and in some cases the former can exceed the latter, as apparently seen in $^{10}-(\text{BEDT-TTF})_2\text{SF}_5\text{CH}_2\text{CF}_2\text{SO}_3$ [31].

At any rate, it appears that electron-electron and electron-phonon interactions are important in quasi-two-dimensional organic superconductors, leading to substantial renormalisations of the quasiparticle masses.

2.5. The pressure dependence of the bandstructure and its effect on superconductivity.

The pressure dependence of the magnetic quantum oscillations has been examined in $-(\text{BEDT-TTF})_2\text{Cu}(\text{NCS})_2$ [20, 71], $-(\text{BEDT-TTF})_2\text{Cu}[\text{N}(\text{CN})_2]\text{Br}$ [72, 73] (see also comments in Reference [74]), $-(\text{BEDT-TTF})_2\text{Cu}[\text{N}(\text{CN})_2]\text{Cl}$ [75] and $-(\text{BEDT-TTF})_2\text{Cu}_2(\text{CN})_3$ [76]. The results from all four materials follow the same general trend, and so we shall illustrate the general features using data from References [20, 71].

Figure 10 shows the resistance of $-(\text{BEDT-TTF})_2\text{Cu}(\text{NCS})_2$ at $T = 0.7\text{ K}$ for several different hydrostatic pressures [20, 71]. A comparison with Figure 6 shows that the increasing pressure suppresses the superconductivity; by $P = 3.1\text{ kbar}$, the critical field is a fraction of a Tesla. At 6.1 kbar there is no evidence of superconductivity at all. However, the Shubnikov-de Haas oscillations due to the hole pocket remain present, so that its k -space area and mass can be extracted as a function of pressure. As the pressure increases, the breakdown oscillations also become visible at much lower magnetic fields [20].

Figure 11 shows the pressure dependence of m_{hole} (corresponding to the hole pocket), m_{orb} (corresponding to the orbit) and the superconducting critical temperature. The application of pressure causes both masses to decrease (see also

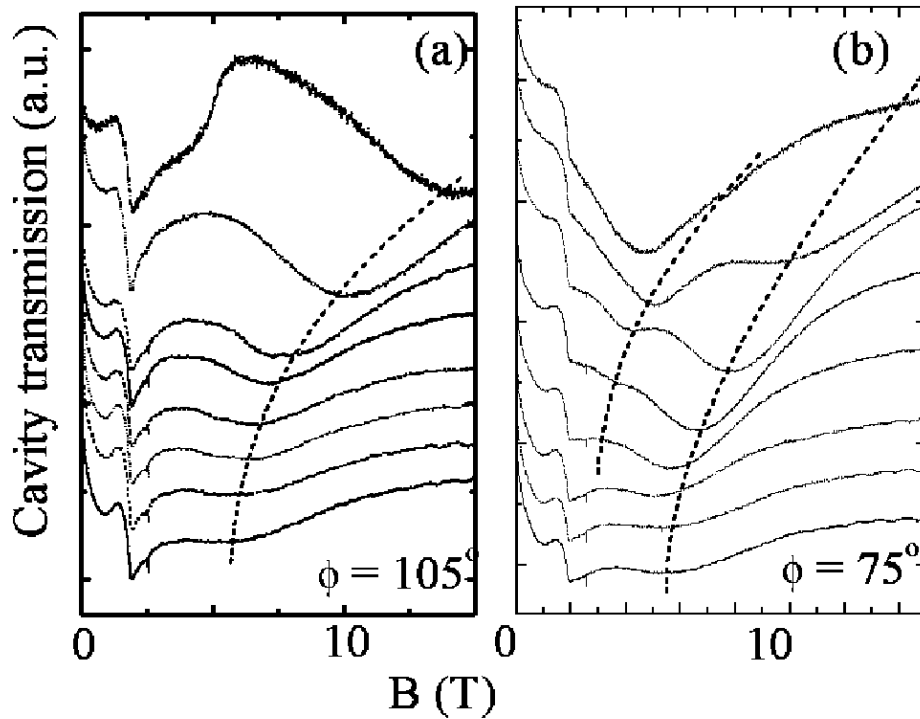


Figure 9. Cyclotron resonance in $\text{Tl}-(\text{BEDT-TTF})_2\text{SF}_5\text{CH}_2\text{CF}_2\text{SO}_3$ (after Reference [31]). (a) Transmission of a resonant cavity loaded with a single crystal of $\text{Tl}-(\text{BEDT-TTF})_2\text{SF}_5\text{CH}_2\text{CF}_2\text{SO}_3$ versus magnetic field for $\phi = 0$ (lowest trace) to $\phi = 105$ (uppermost trace) and $\phi = 105$ ($T = 1.5\text{ K}$). Here ϕ denotes the angle between the normal to the quasi-two-dimensional planes of the sample and the magnetic field; ϕ refers to the plane of rotation of the sample within the magnetic field [31]. (b) Equivalent data for $\phi = 75^\circ$. In both data sets, the structure at low fields is associated with the superconducting-normal transition of $\text{Tl}-(\text{BEDT-TTF})_2\text{SF}_5\text{CH}_2\text{CF}_2\text{SO}_3$, and with a background feature of the cavity. The dotted lines denote movement of the cyclotron resonance (a,b) and its second harmonic (b) only [31]. The azimuthal angle dependence of the harmonic intensity enables the shape of the Fermi surface to be mapped.

Reference [73]). This decrease in effective mass with increasing pressure seems to be a universal feature of the β -phase BEDT-TTF salts; Weiss et al. have shown that the values of m^* for three different β -phase salts map onto a common curve as a function of pressure [73].

The superconducting critical temperature decreases very rapidly as the masses fall; by 5 kbar, T_c is immeasurably small. It is well known that the density of states at the Fermi energy is proportional to the effective mass [20, 24]; as the effective masses fall with increasing pressure, the density of states at the Fermi energy will also decrease. Mechanisms for superconductivity involve the pairing of electrons of equal and opposite k caused by the exchange of virtual excitations such as phonons [78]. The strength of the pairing is directly determined by the rate at which this exchange can take place, which in turn depends on the density of states at the Fermi energy [71]. Thus, the decrease of the

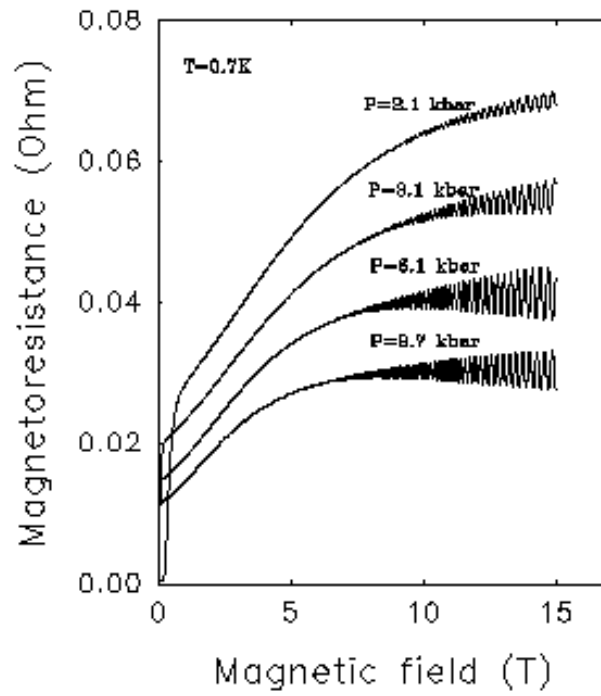


Figure 10. Resistance of $-(\text{BEDT-TTF})_2\text{Cu}(\text{NCS})_2$ at $T = 0.7 \text{ K}$ for several different hydrostatic pressures (after Reference [20]).

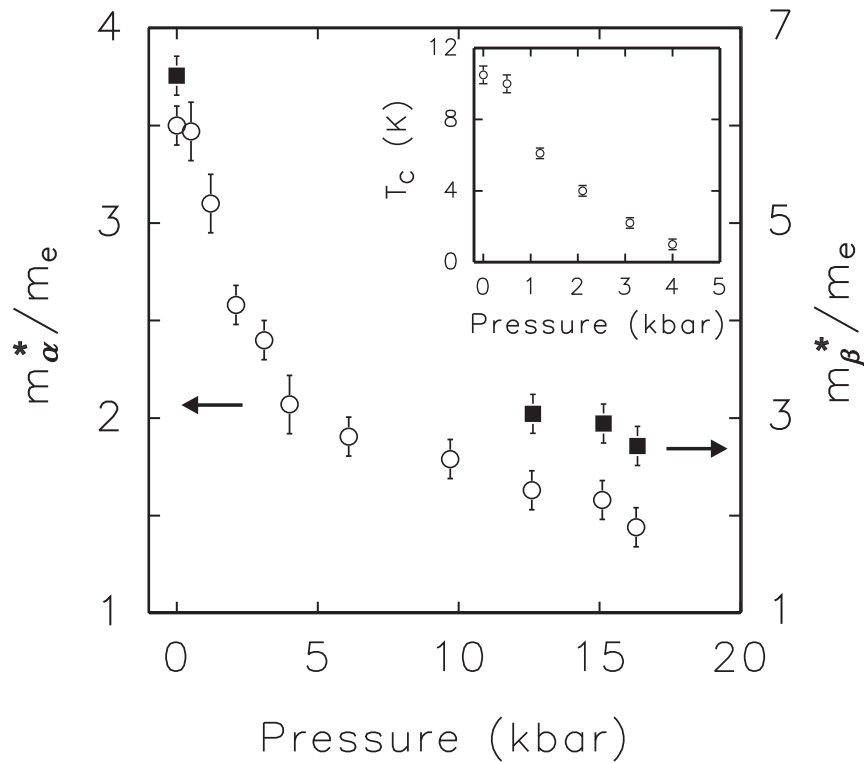


Figure 11. Effective masses of the hole pocket m_α^* and orbital m_β^* as a function of pressure (main Figure). The inset shows the superconducting critical temperature T_c as a function of pressure (after Reference [20]).

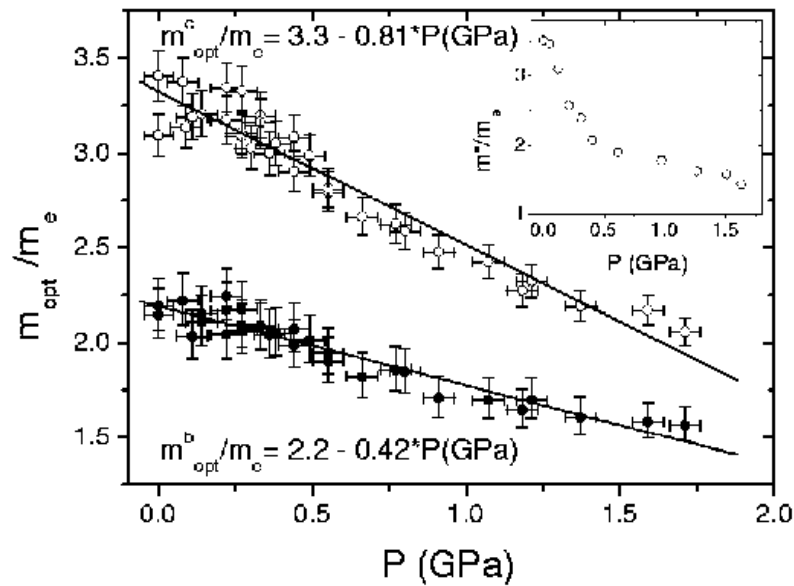


Figure 12. "Optical masses" deduced from reflectivity data as a function of pressure. The variation of the effective mass with pressure from Figure 11 is reproduced in the inset (after Reference [77]).

effective masses reduces the density of states at the Fermi energy, thereby suppressing the superconductivity. Any model of superconductivity should therefore potentially allow one to relate T_c to m^* . Lee solved the linearised Eliashberg equations to get the dependence of T_c on m^* [71, 79] using an Einstein phonon energy of 5 meV (close to a prominent maximum in the phonon density of states) an ambient-pressure electron-phonon coupling constant of 0.4 (c.f. values 0.3–0.5 obtained in Reference [59]) and an ambient-pressure Coulomb pseudopotential $\mu^* = 0.22$. Lee pointed out [79] that "an attractive interaction of high-energy origin must be responsible for the pairing potential, which is parameterised by a large negative Coulomb pseudopotential.... this high-energy interaction... could come from spin fluctuations." Since Lee's work, a number of other authors have noted the importance of spin fluctuations in the α -phase BEDT-TTF salts (see Section 3.1.1).

In order to clarify what is responsible for the reduction in effective mass with pressure, Kake et al. [77] performed reflectivity measurements on a sample of $-(\text{BEDT-TTF})_2\text{Cu}(\text{NCS})_2$ as a function of pressure. They were able to deduce "optical masses" (Figure 12) which are closely related to the bare band mass (see previous section). Although the absolute values of the optical masses are likely to be scaled by some numerical factor [77], their relative shift with pressure is a good guide to what happens to the bare band mass. In contrast to the "elbow-like" variation of the effective mass with pressure (see Figure 11), the optical mass shows a smooth decrease. This indicates that the rapid change in effective mass seen below 5 kbar (0.5 GPa) is associated with a strong decrease in the electron-electron interactions and/or electron-phonon interactions (which contribute to the effective mass but not to the bare band mass; see Section 2.4).

"Chemical pressure", that is, the use of longer anions to stretch the unit cell, can be used to explore what are effectively negative pressures compared to the actual pressures in Figure 11. The most "negative" chemical pressure is achieved with $-(\text{BEDT-TTF})_2\text{Cu}[\text{N}(\text{CN})_2]\text{Cl}$, which is an insulator at ambient (actual) pressure [75, 94]. (This salt is actually what is known as a Mott insulator [13, 24], in which the transfer integrals are small compared to Coulomb repulsion between holes on neighbouring dimers, thus preventing the holes from hopping.) The chemical pressure is less negative for $-(\text{BEDT-TTF})_2\text{Cu}[\text{N}(\text{CN})_2]\text{Br}$ [72, 73], which teeters between insulating and metallic behaviour; as a result, the detailed behaviour of this salt has received considerable attention [80, 81]. We shall return to the effect of pressure and the superconducting phase diagram below (Figure 13).

2.6. The temperature dependence of the resistance.

The normal-state resistivity of the superconducting BEDT-TTF salts varies as T^2 , at least up to temperatures $T \approx 30-40$ K [82]. This is yet another indication that electron-electron interactions are important [24] in quasi-two-dimensional organic superconductors. Above this temperature, the rate of increase in resistivity with temperature slackens off.

At slightly higher temperatures still, the resistivities of the α -phase BEDT-TTF salts tend to exhibit a broad peak or hump. In the case of $-(\text{BEDT-TTF})_2\text{Cu}(\text{NCS})_2$, the hump occurs at about 90 K [83]. Above this temperature, the resistivity of the α -phase salts decreases slowly with increasing temperature (i.e. they have an "insulating"-type behaviour). The hump is usually associated with small rearrangements of the terminal ethylene groups of the BEDT-TTF molecule [83]; however, recent optical data have been used to support the argument that the transition from "insulating" (high T) to "metallic" (low T) behaviour occurring at the hump represents a shift from small polaron to large polaron conduction [123].

At this point it is necessary to add a note of caution about resistivity measurements in quasi-two-dimensional organic conductors. Whilst interlayer resistivity (ρ_{zz}) measurements are simple [84], the very large resistivity anisotropy $\sim 10^3-10^5$ [1] makes quantitative experimental measurements of the intralayer resistivity using conventional wires and contacts almost impossible [84]; there is almost always a substantial component of ρ_{zz} present. Part of the problem stems from the irregular shape and small size of the high-quality single crystals; typical dimensions are $\sim 1 \times 0.5 \times 0.1$ mm [84]; at present, high quality epitaxial films are not available.

Indeed, it is very probable that the only reliable estimates of the intralayer resistivity are those derived from skin-depth (see Reference [29] and references therein) and optical conductivity studies [129].

The term polaron is used to describe an electron accompanied by a strain field (i.e. a distortion of the crystal caused by the electron interacting with polar molecules) [24].

2.7. Summary of Fermi-surface and quasiparticle properties

In the following sections, we shall describe what is known about the superconducting state of quasi-two-dimensional (quasi-two-dimensional) organic superconductors. It is therefore a convenient point to summarise all that has been discussed about the normal-state properties thus far.

- (i) The organic superconductors described in this review are charge-transfer salts, comprising bandstructure-forming cation molecules Y (Y is BEDT-TTF, BETS, BEDO etc.) and anion molecules X ; n Y molecules jointly donate an electron to X , stabilising the charge-transfer salt Y_nX and leaving behind a hole.
- (ii) The band-structure-forming molecules pack into layers, separated by layers of anion molecules. The bandshape and bandwidth can be altered chemically by changing the anion. The various structural morphologies available are denoted α , β , γ , δ , etc..
- (iii) The layered nature of the salts results in a quasi-two-dimensional bandstructure. The extensive application of techniques such as the de Haas-van Alphen effect, angle-dependent magnetoresistance oscillations and the Fermi-surface traversal resonance means that the intralayer Fermi-surface topology is often known to good accuracy [1].
- (iv) The interlayer transfer integrals of quasi-two-dimensional organic superconductors are very small (~ 0.5 – 2 Kelvin). Nevertheless, many appear to exhibit unambiguous experimental signatures of a three-dimensional Fermi surface.
- (v) Many-body effects are quite pronounced, leading to a Fermi-liquid picture in which the quasiparticle effective mass can be several times larger than the bare band mass.

3. The superconducting state; mechanism for superconductivity

A discussion of the superconducting state of quasi-two-dimensional organic conductors is complicated by apparently contradictory experimental evidence. Most has been done on the α -phase BEDT-TTF salts, and at first (in the early to mid 1990s) it was frequently assumed that their superconductivity could be described by a Bardeen-Cooper-Schrieffer (BCS)-like model. It was assumed that the order parameter was roughly isotropic (s -wave-like); at the time, data from several experiments seemed not inconsistent with this interpretation (see e.g. References [20, 85, 86, 87]). Subsequently, considerable doubt was cast on this idea [88], with the greater proportion of more recent experimental

] The Bardeen-Cooper-Schrieffer (BCS) theory envisages pairing between quasiparticles of equal and opposite momentum and spin, with the pairing interaction being communicated by the exchange of a virtual phonon (lattice vibration). As a result, an energy gap of size 2Δ , where Δ is known as the order parameter, opens up around E_F , separating the paired states from the normal quasiparticles. In the BCS model this energy gap is uniform over all the Fermi surface (this is known as an s -wave-type order parameter). The BCS theory appears to describe elemental superconductors and many alloys very adequately [24].

data suggesting that these salts exhibit a d-wave order parameter (with nodes), the superconductivity being mediated by antiferromagnetic fluctuations. In this context, the nodes are regions over which the order parameter (and energy gap) becomes zero; d-wave refers to the likeness of the node and antinode arrangement to atomic d orbitals.

However, the situation is not quite resolved, as a number of other experiments suggest a completely gapped superconducting state [89, 90]. Moreover, infrared reflectivity and Raman data present a plethora of results and interpretation suggesting that electron-phonon interactions, antiferromagnetic fluctuations and perhaps other electron-electron interactions are all important (or at least in some way involved) in the mechanism for superconductivity, although the details remain unclear, and in some cases the interpretations are divergent.

Most of the more recent experiments have been carried out on the β -phase BEDT-TTF salts. We shall treat these results in some detail, giving a summary of the behaviour of the β -phase salts in Section 3.6.

3.1. The β -phase BEDT-TTF salts; evidence in favour of d-wave and gap nodes.

3.1.1. Proximity of superconductivity to antiferromagnetism; NMR experiments. Initial proposals for non-phonon-mediated superconductivity in the β -phase BEDT-TTF salts were prompted by similarity between their phase diagrams and those of the high- T_c cuprates and heavy-fermion compounds [1, 2, 91] (see Figure 13). It is important that in all cases, the superconducting region of the phase diagram is in close proximity to antiferromagnetism, suggesting that antiferromagnetic fluctuations are important in the superconducting mechanism.

Such proposals gain some of their strongest support from nuclear magnetic resonance (NMR) measurements. Relaxation rates ($1/T_1$) and Knight shifts carried out by three independent groups [95, 96, 97] show behaviour reminiscent of the high- T_c cuprates, in which antiferromagnetic phase fluctuations and spin-gap behaviour dominate; the Hebel-Slichter peak, a feature expected for fully gapped (BCS-like) superconductors, is absent [95, 96, 97] (see Reference [88] and References therein for a general comparison of the NMR properties of the β -phase BEDT-TTF salts with those of other materials). In the superconducting state, it has been stated that the NMR data "rule out the BCS electron-phonon mechanism as the source of the superconductivity, but support an unconventional pairing state with possible nodes in the gap function" [95]; similar comments are made in References [96, 97], based on the observation that the ^{13}C NMR spin-lattice relaxation rate varies approximately as T^3 .

The most recent NMR studies are also the most detailed. Lefebvre et al. carried out NMR and simultaneous ac susceptibility studies of single crystals of β -(BEDT-TTF) $_2\text{Cu}[\text{N}(\text{CN})_2]\text{Cl}$ within a hydrostatic helium gas-pressure cell [81]. The phase diagram deduced is shown as Figure 14.

As has been mentioned above, at low pressures, this salt is an insulator. Below 25 K, the magnetic moments of the conduction holes become ordered into an antiferromagnetic

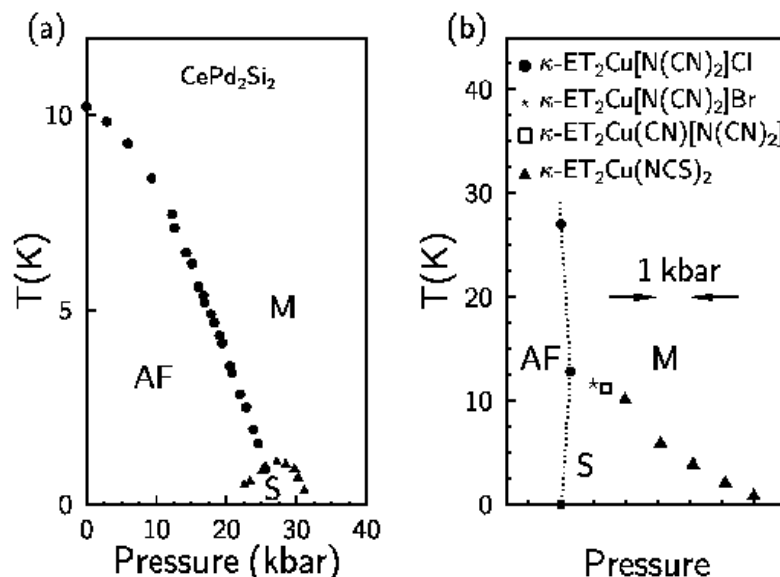


Figure 13. An illustration of the similarity between κ -phase BEDT-TTF superconductors and heavy-fermion compounds. (a) Temperature-pressure phase diagram of the heavy fermion superconductor CePd_2Si_2 (after Reference [92]). (AF = antiferromagnetism, S = superconductivity, M = metal) (b) Temperature-pressure phase diagram of the organic superconductors $\kappa\text{-(BEDT-TTF)}_2\text{Cu}(\text{NCS})_2$, $\kappa\text{-(BEDT-TTF)}_2\text{Cu}[\text{N}(\text{CN})_2]\text{Br}$, $\kappa\text{-(BEDT-TTF)}_2\text{Cu}(\text{CN})[\text{N}(\text{CN})_2]$ and $\kappa\text{-(BEDT-TTF)}_2\text{Cu}[\text{N}(\text{CN})_2]\text{Cl}$. The pressure axis includes the effect of "chemical pressure" caused by chemically varying the unit cell size (see Section 2.5) as well as conventionally applied hydrostatic pressure; the lines indicate the ambient-pressure positions of the three named substances (adapted from References [20, 91, 81, 3]). Note that the left-hand region of the phase diagram is somewhat simplified for clarity [93]; see Figure 14 [81] (after Reference [1]).

(AF) state; in other words, alternate holes, each localised on a dimer (pair of molecules—see Figure 2), have opposite spin. As the temperature rises, the magnetic order disappears, and the system is a paramagnetic insulator (PI).

On increasing the pressure, the high-temperature phase of $\kappa\text{-(BEDT-TTF)}_2\text{Cu}[\text{N}(\text{CN})_2]\text{Cl}$ becomes metallic (M); in other words the holes are free to move about the crystal, conducting electricity. At low temperatures, the increases of pressure result in unconventional superconductivity (U-SC). Over a restricted region (shaded), there is an inhomogeneous phase within which superconductivity coexists with regions of antiferromagnetism.

The intersection of the metal-insulator (MI) boundary with the Neel temperature, $T_N(P)$, at $(P; T)$ is of great interest, since it shows the absence of a boundary between the metallic and antiferromagnetic (AF) phases. This confirms suggestions about the absence of itinerant antiferromagnetism in κ -phase BEDT-TTF salts [91] and the relevance of a description of magnetic ordering in terms of interacting spins localized on dimers [91, 98]. In other words, the antiferromagnetic interactions are

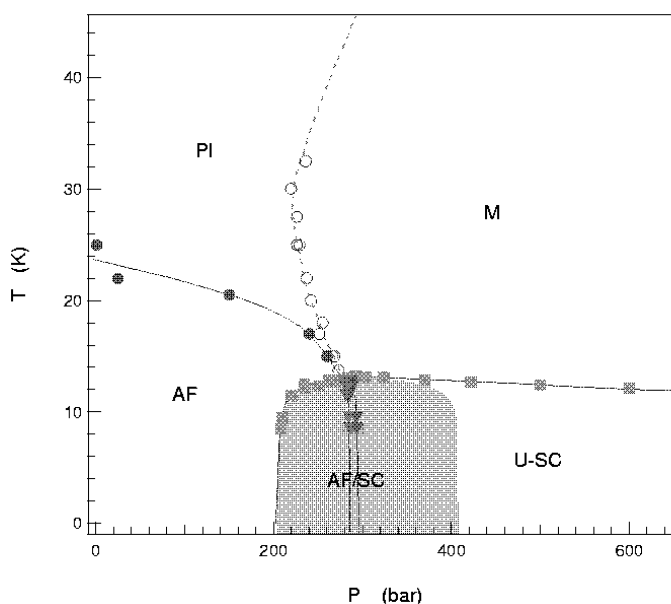


Figure 14. Temperature versus pressure phase diagram of $-(\text{BEDT-TTF})_2\text{Cu}[\text{N}(\text{CN})_2\text{Cl}]$ [81]. The antiferromagnetic (AF) critical line $T_N(P)$ (dark circles) was determined from NMR relaxation rate while $T_C(P)$ for unconventional superconductivity (U-SC: squares) and the metal-insulator $T_{M-I}(P)$ (MI: open circles) lines were obtained from the AC susceptibility. The AF-SC boundary (double dashed line) separates two regions of inhomogeneous phase coexistence (shaded area).

associated solely with the bands derived from the BEDT-TTF molecules, and not in any way related to the Cu present in the anions [5]. The fact that superconducting (SC) and AF phases overlap below P^* indicates that superconductivity can be directly stabilized from the insulating phase, a phenomenon noted in studies of other BEDT-TTF superconductors [99].

Further support for the importance of antiferromagnetic fluctuations has emerged from theoretical calculations which are able to predict the behaviour of $1/T_1$ as a function of temperature [47]. Similarly, using a two-band description of the antibonding orbitals on a BEDT-TTF dimer and an intermediate local Coulomb repulsion between two holes on one dimer, Schmalian [5] was able to determine the magnetic interaction and superconducting gap functions of a typical α -phase BEDT-TTF salt within the fluctuation-exchange approximation (see also References [98, 4]). Schmalian [5] found that the pairing interaction within this model is determined by interband coupling, additionally affected by spin excitations of the quasi-one-dimensional Fermi-surface sections; moreover, he was able to predict superconducting transition temperatures $T_C \approx 10$ K, close to those observed experimentally. The predictions for the shape of the order parameter within Schmalian's model are shown in Figure 15.

3.1.2. Direct measurements of the anisotropic order parameter. Direct evidence for the anisotropic nature of the superconducting order parameter in $-(\text{BEDT-TTF})_2\text{Cu}[\text{N}(\text{CN})_2\text{Cl}]$ is provided by the observation of a

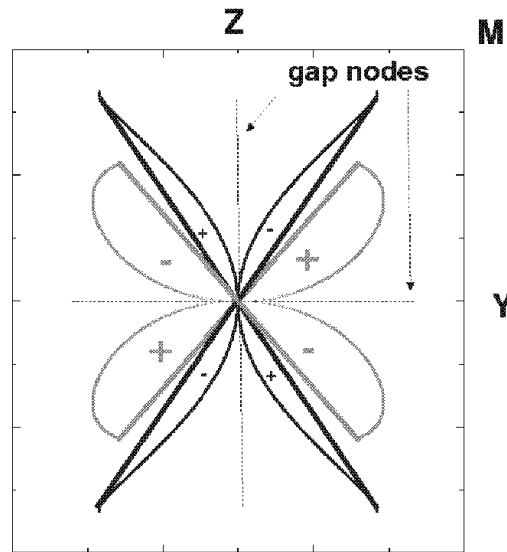


Figure 15. Polar plot of the superconducting gap functions of the two bands (i.e. quasi-one-dimensional and quasi-two-dimensional) at the Fermi surface of $-(\text{BEDT-TTF})_2\text{Cu}(\text{NCS})_2$, calculated by Schmalian [5]. The amplitude of the gap corresponds to the distance from the origin. Gap nodes occur along the y and z directions; additional suppression of the gap along the diagonal is caused by the gap between quasi-one-dimensional and quasi-two-dimensional Fermi surface (compare Figure 5 (a)).

$\text{TTF})_2\text{Cu}(\text{NCS})_2$ has come from scanning-tunnelling microscopy (STM) studies of single crystals at low temperatures [100]. Figure 16 shows typical data; it is fairly obvious from the raw data that the (dI/dV) curves are quite strongly affected by the in-plane tunnelling direction (defined in the Figure by the angle ϕ). Such data have been fitted to d-wave gap models with some success, yielding maximum gap values $2\Delta_0 = k_B T_c \approx 6.7$, substantially larger than the BCS value of 3.53 [100]. However, in contrast to the predictions of Schmalian [5], the STM data appear to favour nodes directed at 45° to the k_B axis, i.e. rotated by $\pi/4$ compared to those shown in Figure 15.

This contradiction seems to have been resolved very recently by new calculations of Kuroki et al., who showed that the orientation of the calculated node pattern was rather critically dependent on the fine details of the bandstructure [101]. By choosing suitable parameters, Kuroki et al. were able to reproduce the node orientation observed in the STM experiments.

An attempt has also been made to observe the gap nodes in $-(\text{BEDT-TTF})_2\text{Cu}(\text{NCS})_2$ using GHz conductivity measurements [102]. However, although these data also suggest an anisotropic gap, their interpretation remains controversial [103].

yyIn this context it should be noted that the transfer integrals used by Schmalian as input parameters for his calculation [5] differ somewhat from more recent, accurate values [21].

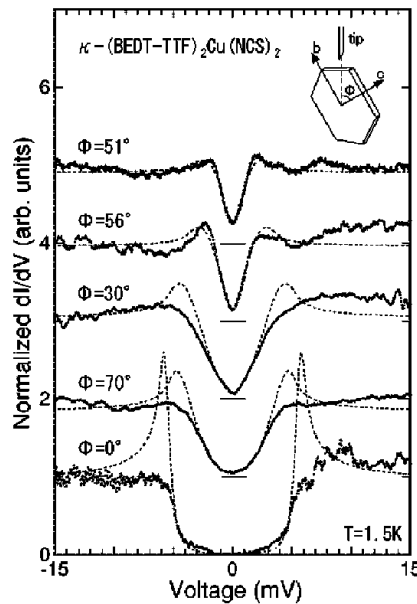


Figure 16. (dI/dV) data obtained in tunnelling experiments on the lateral surfaces of a κ -(BEDT-TTF) $_2$ Cu(NCS) $_2$ single crystal (solid lines; $T = 1.5$ K). The inset shows the definition of the angle Φ used to denote the tunnelling direction. The dashed curves are a fit to a d-wave gap model (after Reference [100]).

3.1.3. Penetration-depth, Muon Spin Rotation and thermal conductivity measurements. More recent penetration depth measurements in the superconducting state of the κ -phase BEDT-TTF salts also seem to support a d-wave picture. Early studies [85, 86] were complicated by difficulties associated with vortex dynamics (see References [104, 105, 106] for a discussion); in more recent work [105, 106, 108], the importance of neutralising the influence of external fields has been realised, and very large values of the penetration length for magnetic fields in the highly-conducting planes of κ \sim 100 microns [105, 108] and \sim 0.2 mm [106] have been found; millimetre-wave studies [109, 110] are in broad agreement with these findings. In all of these studies, the penetration depth shows a non-BCS-like behaviour as a function of T , leading to statements such as "our measurements give strong evidence for... low-lying excitations...; values of λ_J are significantly closer to those required for d-wave superconductivity" [105] and "magnetic field penetration depth results... indicate an anisotropic superconductivity of a gapless nature" [106].

Initial muon-spin rotation (SR) [107] studies of κ -phase BEDT-TTF salts gave inconclusive results because of the complex vortex dynamics; Reference [104] shows that earlier, apparently definitive statements about the nature of the superconductivity in BEDT-TTF salts are based on over-simplified analysis. Subsequently, more sophisticated analysis of the temperature dependence of SR data appears to favour a superconducting gap with nodes [112].

The presence of nodes is also suggested by measurements of the thermal conductivity [111], which is proportional to T below the superconducting critical

temperature T_c . Finally, it has been remarked that the sensitivity of T_c to disorder in the π -phase BEDT-TTF salts points to a non-BCS mechanism for superconductivity [113].

3.2. The π -phase BEDT-TTF salts; evidence against gap nodes.

The chief evidence against gap nodes has come from heat capacity measurements by the group of Wosnitzer [89]. Typical data are shown in Figure 17 for π -(BEDT-TTF)₂Cu[N(CN)₂Br]; the experiments compare the heat capacity measured in zero magnetic field (superconducting) and at $B = 14$ T (normal). The difference between the measured heat capacities at $B = 0$ and $B = 14$ T (Figure 17, right-hand side), attributed to the superconductivity, appears to follow a BCS, strong-coupling-like temperature dependence, implying a fully-gapped superconducting state.

It is interesting to speculate as to why the heat capacity data should imply such a different superconducting groundstate from the other experimental probes. Discussion on this matter has encompassed experimental difficulties, including the possible field dependence of the thermometry used [114], the extreme difficulty in subtracting the other contributions to the heat capacity, the presence of other field-dependent contributions to the heat capacity [114, 115] and the evolution of the form of the superconducting order parameter with magnetic field [116]. At present, the matter is unresolved.

3.3. The isotope effect.

The isotope effect [24] was a key piece of evidence for the BCS (phonon-mediated) model of superconductivity. It was found that the superconducting critical temperature of a particular isotope of an elemental superconductor was often proportional to $M^{-1/2}$, where M is the isotopic mass. This is a strong indication that phonons are providing the basic energy scale for the superconductivity; if phonons are regarded as oscillations of an array of masses (the atoms or molecules) on "springs" (the chemical bonds—see References [16, 24]), then the characteristic phonon energy should scale as $M^{-1/2}$. The absence of an isotope effect or the presence of an anomalous isotope effect are suggestive of a non-BCS-like mechanism for superconductivity.

Workers at Argonne National Laboratories have made very careful studies of the isotope effect. These show only very small influences of the molecular mass on T_c [117]; in some cases (replacement of the 8^1H in BEDT-TTF with 2^2H) a "negative isotope effect" was observed, whereas a very small shift of T_c in the expected direction was seen when S and C atoms were substituted with heavier isotopes [117]. These data could signal support for either phonon-mediated or more exotic forms of superconductivity [117]. One of the effects of deuteration may be to change the length of the C-H bonds on the ends of the BEDT-TTF molecule [117]. Therefore, deuteration is analogous to the effects of anisotropic expansion [118] and/or pressure; both the phonon system and the electronic system (see Sections 2.5 and 3.1.1) are likely to be affected [77]. This matter at present therefore remains inconclusive.

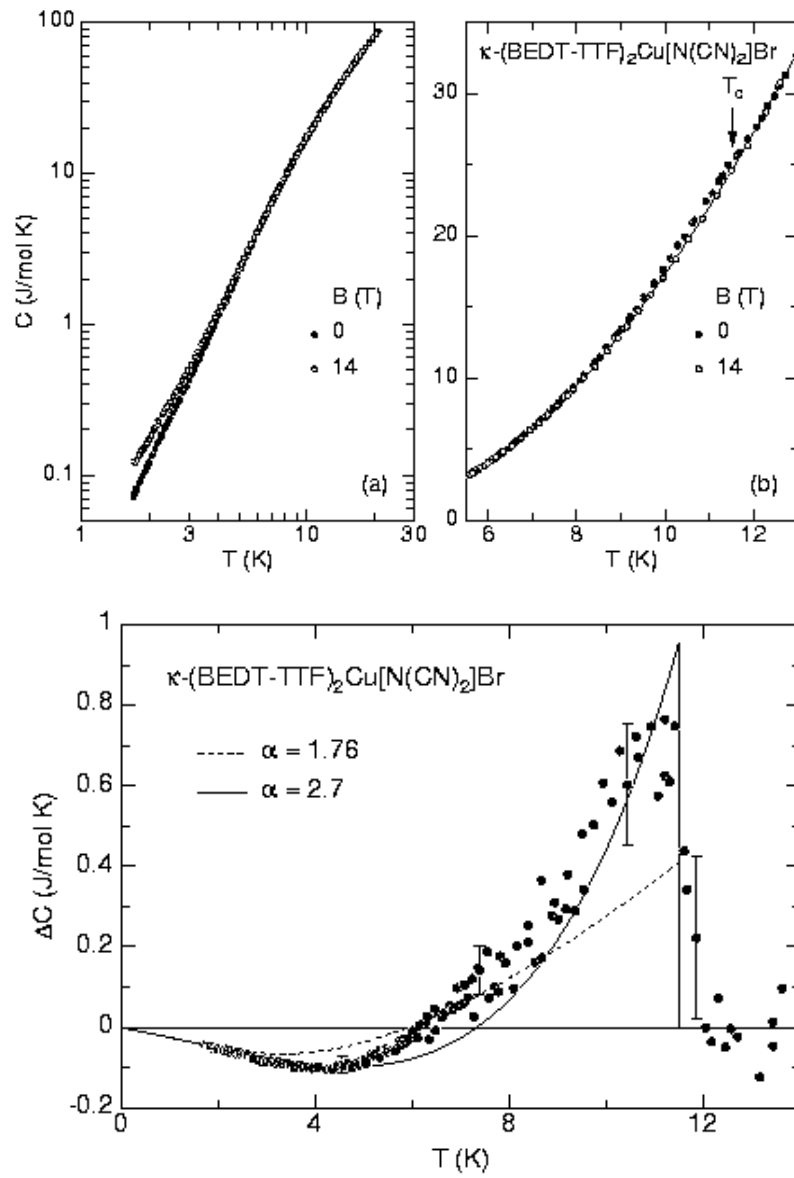


Figure 17. Temperature dependence of the specific heat of κ -(BEDT-TTF)₂Cu[N(CN)₂]Br in the superconducting ($B = 0$) and normal ($B = 14$ T) state shown (left) for the complete temperature range and (right) for the region close to $T_c = 11.5$ K. The solid line in the centre figure is a polynomial fit to the 14 T data. Bottom: specific heat difference between the superconducting ($B = 0$) and normal state ($B = 14$ T) with theoretical BCS curves for weak (dashed line) and strong (solid line) coupling (after Reference [89]).

3.4. Raman scattering and infrared measurements; the role of phonons

3.4.1. Experimental data and interpretation Raman scattering and infrared reflectivity have been used extensively in studying quasi-two-dimensional organic superconductors. There are several good motivations for examining the infrared reflectivity; (i) reflectivity can potentially probe low-energy excitations which are characteristic of the bare, undressed, band electrons [60] (see Sections 2.4 and 2.5); (ii) models (e.g. Reference [119]) can be used to obtain an indication of phonon-specific electron-phonon interactions [120] from reflectivity data; (iii) the mid-infrared reflectivity of organic molecular metals exhibits a large hump, which has been interpreted as a direct measure of the Coulomb correlation energy [121]. Thus, infrared studies potentially enable effects due to the bare bandstructure, the electron-phonon interactions and the electron-electron interactions to be distinguished [120, 122].

Figures 18 and 19 show typical data, either as raw reflectivity (Figure 18 (a) and (b)) or as conductivity derived from the reflectivity [77, 123]. Note the presence of the broad hump around 3000 cm^{-1} mentioned above, the sharp lines due to phonons and the low-frequency conductivity, which increases as the temperature is lowered (Figure 18 (c), (d)) and/or the pressure is raised (Figure 19). The latter feature is interpreted as a Drude [24] peak (see References [77, 123] and references therein), which becomes more prominent as the material's metallic character increases with increasing pressure or decreasing temperature.

The interpretation of reflectivity data from the α -phase BEDT-TTF salts is still somewhat varied. For example, Wang et al. argue quite convincingly that data such as those in Figure 18 are best understood in terms of polaron absorption (see Reference [123] and references therein). The broad hump, most prominent at high temperatures, is interpreted as photon-assisted hopping of small polarons (c.f. Reference [121]); the sharp Drude peak that develops at low temperature together with spectral weight in the mid infrared are attributed to coherent and incoherent bands of small polarons. Thus, Wang et al. associate the transition from insulating-like behaviour at high temperature to metallic behaviour at low temperature (Section 2.6) with a crossover from localised small polarons to coherent large polarons [123].

Klehe et al. interpret their pressure-dependent reflectivity differently, but were able to extract optical quasiparticle masses by integrating over the whole of the measured optical conductivity [77]. The measured optical mass shows a small linear pressure dependence (Figure 12), in contrast to the rapidly-varying effective mass m^* shown in Figure 11. As the optical mass is closely related to the bare band mass (see Sections 2.4 and 2.5), this implies that the rapid variation of m^* with pressure is associated with significant changes in the interactions which renormalise the quasiparticle mass [77]. By comparing their reflectivity data with Raman experiments as a function of pressure [130, 131], Klehe et al. suggest that it is the electron-electron

An introduction to Raman scattering at a good, basic level is given in *Optical properties of solids*, by Mark Fox (Oxford University Press, 2001).

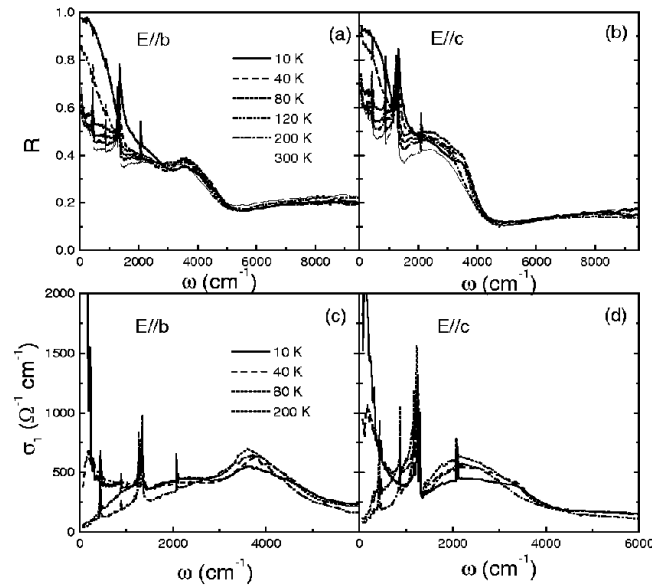


Figure 18. Reflectivity of $-(\text{BEDT-TTF})_2\text{Cu}(\text{NCS})_2$ as a function of photon energy for infrared polarised parallel b (a) and c (b) respectively. Data for several temperatures are shown. (c) and (d) show the corresponding frequency-dependent conductivity, σ_r (after Reference [123]). Note the sharp peaks due to phonons and the increase in low-frequency conductivity (i.e. metallic behaviour) as the temperature decreases.

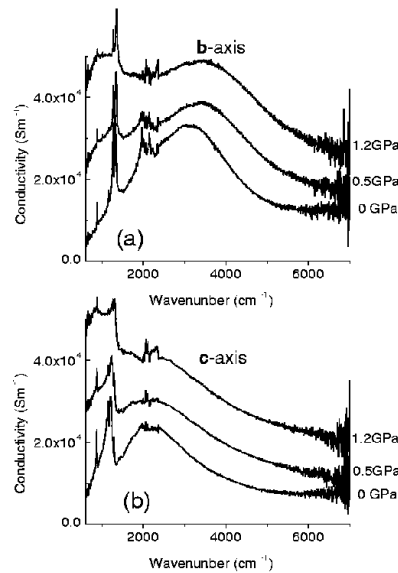


Figure 19. Room temperature frequency-dependent conductivity σ_r of $-(\text{BEDT-TTF})_2\text{Cu}(\text{NCS})_2$ for infrared polarised parallel to b (top) and c (bottom) for pressures 0, 0.5 and 1.2 GPa (after Reference [77]). Note the increase in low-frequency conductivity as the pressure increases.

interactions which are most important in determining the pressure dependence of the superconductivity.

A number of Raman studies of β -phase BEDT-TTF salts are reviewed and compared with those on high T_c cuprates in Reference [90], which also reports a microRaman study of low-frequency (energies less than 100 cm^{-1}) phonon modes in $-(\text{BEDT-TTF})_2\text{Cu}[\text{N}(\text{CN})_2]\text{Br}$. This particular paper is interesting because phonon self-energy effects are monitored as the salt enters its superconducting phase; the resulting energy shifts are interpreted in terms of a strong-coupling BCS model (i.e. fully-gapped), yielding an electron-phonon coupling constant $\lambda = 0.97$ [90]. Analogous Raman data involving higher-frequency phonons ($500 - 1500 \text{ cm}^{-1}$) were reported by Eldridge et al., who observed a shift of surprisingly high-energy phonons (i.e. energies much greater than $k_B T_c$) at T_c [124]. Eldridge et al. speculated that the normal electron-phonon interaction may not be responsible for the frequency change, but that the superconducting transition may involve a change in either the geometry or the arrangement of the BEDT-TTF molecules to which the particular mode is sensitive [124]. (Reference [124] is also notable as a good survey of earlier Raman studies.)

Finally, infrared and Raman measurements also show evidence for the coupling of antiferromagnetic fluctuations to phonons which are suspected of involvement in the superconductivity [125, 126]. Some representative data are shown in Figure 20, which shows the normalised frequency of the ν_g (A_g) mode in $(\text{BEDT-TTF})_2\text{I}_3$, $-(\text{BEDT-TTF})_2\text{AuI}_2$, $-(\text{BEDT-TTF})_2\text{Cu}[\text{N}(\text{CN})_2]\text{Br}$ and $-(\text{d8-BEDT-TTF})_2\text{Cu}[\text{N}(\text{CN})_2]\text{Br}$ as a function of temperature; in the latter material, the eight terminal hydrogens have been replaced with deuterium. For $(\text{BEDT-TTF})_2\text{I}_3$ and $-(\text{BEDT-TTF})_2\text{AuI}_2$, the usual hardening (increase in frequency) of the mode occurs as the lattice contracts with decreasing temperature. However, in the case of the two β -phase salts, softening (reduction in frequency) occurs below the temperature at which antiferromagnetic fluctuations, measured in NMR studies [126], become important [126]. Note that $(\text{BEDT-TTF})_2\text{I}_3$ has no antiferromagnetic fluctuations present [126].

3.4.2. Summary of optical data To summarise the optical data, it must be said that the picture emerging from infrared and Raman experiments is still unclear. The interaction between the phonon system and antiferromagnetic fluctuations does seem to be important for superconductivity in the β -phase BEDT-TTF salts [126]. However, whereas some interpret their data in terms of a strong-coupling, fully-gapped BCS picture, with an electron-phonon coupling constant $\lambda \approx 1$ [90], others are able to use optical data and ab-initio calculations (see e.g. References [59, 127] and references therein for a review and discussion) to derive values $\lambda \approx 0.3$. Similarly, infrared measurements [128] have been taken to suggest that "intramolecular vibrations are not directly involved in the superconductivity mechanism" and that the electron-phonon coupling constant is small; others found "no evidence that higher values of T_c are achieved through a softer lattice" (i.e. that intramolecular vibrations are not involved in a simple, BCS-like manner) and that the superconductivity "is likely to be a much

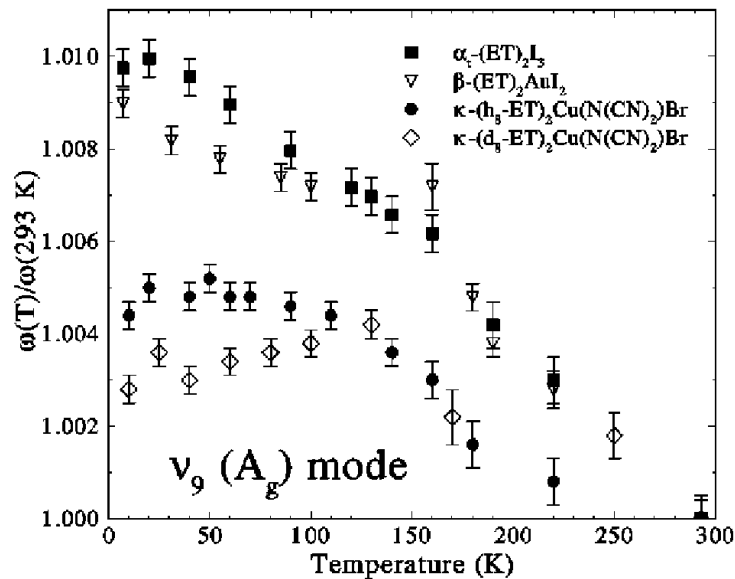


Figure 20. Normalised frequency of the ν_g (A_g) mode in $(\text{BEDT-TTF})_2\text{I}_3$, $-(\text{BEDT-TTF})_2\text{AuI}_2$, $-(\text{BEDT-TTF})_2\text{Cu}[\text{N}(\text{CN})_2]\text{Br}$ and $-(\text{d8-BEDT-TTF})_2\text{Cu}[\text{N}(\text{CN})_2]\text{Br}$ as a function of temperature; in the latter material, the eight terminal hydrogens have been replaced with deuterium. For $(\text{BEDT-TTF})_2\text{I}_3$ and $-(\text{BEDT-TTF})_2\text{AuI}_2$, the usual hardening (increase in frequency) of the mode occurs as the lattice contracts with decreasing temperature. However, in the case of the two κ -phase salts, softening (reduction in frequency) occurs below the temperature at which antiferromagnetic fluctuations become important (after Reference [126]).

more complicated situation than that described by "simple BCS" [129]. The latter view is in part supported by the interpretation of pressure-dependent infrared and Raman data [77, 130, 131], which seems to suggest a dominant role for electron-electron interactions.

These divergent opinions may well reflect as-yet inadequate interpretative tools (see e.g. Reference [132] for a discussion). In spite of this disagreement, it is clear that the optical measurements do suggest important roles for phonons, antiferromagnetic fluctuations and/or other electron-electron interactions in the superconductivity of κ -phase BEDT-TTF salts.

3.5. The role of effective dimensionality.

We have seen above that antiferromagnetic spin fluctuations are not the only important ingredient in superconductivity in the κ -phase BEDT-TTF salts; we also described good evidence that the phonon and magnetic systems interact, perhaps suggesting that the superconducting mechanism in BEDT-TTF salts may involve both phonons and spin fluctuations [71, 79, 125, 133]. In this context, it is interesting to contrast the behaviour of the κ -phase BEDT-TTF salts with the isostructural superconductor $(\text{MDT-TTF})_2\text{AuI}_2$ ($T_c = 4.2 \text{ K}$) [134]. In NMR studies of $(\text{MDT-TTF})_2\text{AuI}_2$, a Hebel-

Slichter peak suggestive of conventional BCS-type superconductivity was observed [135]; furthermore, the specific heat capacity of this material was unambiguously BCS-like [134].

A possible explanation for this difference comes from the anisotropy of the upper critical field in $(\text{MDT-TTF})_2\text{AuI}_2$, which shows [134] that the interlayer coupling is much larger than in β -phase BEDT-TTF superconductors. Models for superconducting pairing mediated by antiferromagnetic fluctuations are sensitive to the degree to which the Fermi-surface may nest [4, 5, 98]; the increased "three dimensionality" of $(\text{MDT-TTF})_2\text{AuI}_2$ may be enough to ensure that required degree of nesting is not present, ruling out this mechanism of superconductivity. It is interesting to speculate about a systematic study of isostructural superconductors with different cations, in which a transition from BCS-like superconductivity to a less conventional mechanism could be engineered.

3.6. The β -phase BEDT-TTF salts.

In many respects the behaviour of the β -phase BEDT-TTF salts is somewhat similar to that of the α -phase salts. For example, NMR studies indicate the lack of a Hebel-Slichter peak, suggesting non-BCS-like superconductivity [136]. Support for a more exotic species of superconductivity also comes from tunnelling experiments, which give maximum energy gap values for β -(BEDT-TTF) $_2\text{AuI}_2$ which are almost four times larger than expected from BCS theory [137]. Nevertheless, as in the case of the α -phase salts, recent calculations for β -phase salts, based on optical data [138], also suggest an important role for phonons in the mechanism for superconductivity.

There may be one important difference between the α and β -phase salts. Measurements of the electronic susceptibility as a function of pressure in the latter materials seem to show that a variation in the density of states is not a major influence on the superconducting T_c [139] (c.f. the data described in Section 2.5).

3.7. The nature of superconductivity in organics; a summary

In summary, the following remarks may be made.

The greater proportion of experimental techniques (NMR, tunnelling, SR, penetration-depth measurements, thermal conductivity) support a non-BCS (i.e. unconventional) mechanism for superconductivity in the organics.

The data suggest a d-wave order parameter arrangement, with nodes directed along the x and y intraplane directions. NMR studies suggest the involvement of antiferromagnetic fluctuations.

Theoretical calculations invoking the involvement of antiferromagnetic fluctuations are able to reproduce the node pattern and simulate superconducting transition temperatures of a reasonable size.

The interpretation of isotope effect and heat capacity data is unclear at the moment. Differences in interpretation of resistivity and Raman data have also resulted in apparently conflicting statements about the nature of the superconductivity in the organics, whilst nevertheless supporting the involvement of antiferromagnetic fluctuations.

4. The superconducting phase diagram

4.1. The broadened transition and the hump.

In spite of the fact that organic superconductors are rather clean systems (e.g. the intralayer mean-free path in a typical sample of $-(\text{BEDT-TTF})_2\text{Cu}(\text{NCS})_2$ is 2000 \AA [21]), the transition from normal to superconducting seems to be rather broad, whatever the method used. Figure 21 shows the result of a typical zero-magnetic-field experiment; in this case a $-(\text{BEDT-TTF})_2\text{Cu}(\text{NCS})_2$ sample (mean-free-path 2000 \AA) was placed in a coil forming part of a tank circuit oscillating at 38 MHz . The superconducting to normal transition is seen as a change in frequency, caused by a change from skin-depth-limited to penetration-depth-limited coupling of the sample to the MHz fields [29, 140]. The high-temperature onset of the transition is seen as a deviation from behaviour characteristic of the normal state close to 11.0 K ; at low temperatures, the frequency starts to deviate from behaviour characteristic of the superconducting state just below 8 K , so that the total width of the transition is around 3 K . Even if one employs more conventional definitions of the width of the transition [140] (see Figure 21, caption), the transition is still between 0.7 K and 1 K wide (Figure 21). The intrinsic breadth of the transition is almost certainly responsible for the wide range of T_c s quoted for salts such as $-(\text{BEDT-TTF})_2\text{Cu}(\text{NCS})_2$.

How can the transition be so wide in such a clean material? The reason is perhaps associated with the exceptionally two-dimensional nature of the superconductivity. Let us suppose that there are variations in the local potential caused by defects etc.. In a three-dimensional superconductor, the effects of such variations (e.g. on the local density of states) will be averaged over a volume given roughly by ξ^3 , where ξ is the coherence length. On the other hand, in a two dimensional superconductor, the variations will be averaged over an area ξ^2 , corresponding to a much smaller number of unit cells sampled. This means that the effect of the variations is statistically much more significant in two-dimensional materials. Using such an approach, it has been possible to obtain good estimates of the broadening of the transition in $-(\text{BEDT-TTF})_2\text{Cu}(\text{NCS})_2$ [140], based on a density of spatial variations extracted from de Haas-van Alphen oscillations.

In a magnetic field, the situation becomes rather worse, especially in the case of resistive measurements. Figure 6 has already shown that there is a "hump" in the

The resistive onset often appears to occur around 10.4 K , and this temperature is regularly quoted as T_c ; see e.g. Reference [8]. Figure 21 shows that a preferable value would be around 9.5 K .

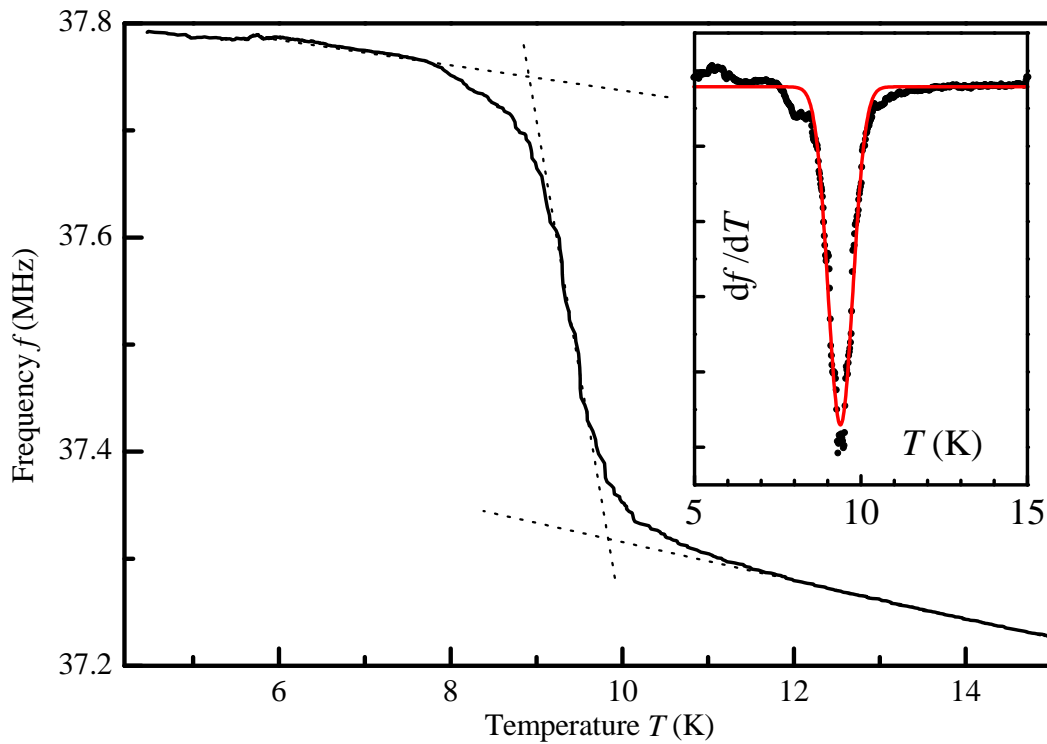


Figure 21. MHz penetration data for a single crystal of $-(\text{BEDT-TTF})_2\text{Cu}(\text{NCS})_2$, shown as resonant frequency f versus temperature T . The superconducting transition is the steeply sloping region between the more gentle variations characteristic of superconductivity (low T) and the normal state (high T); note that the complete transition region occupies a temperature range from around 8 K to 11 K. The dotted lines are extrapolations of the normal-state, transition-region and superconducting-state behaviour. The intersections of the extrapolations occur at 8.9 T and 9.8 T, giving $T_c^{\text{linear}} = 9.35$ K (midpoint) and $T_c^{\text{linear}} = 9.09$ K. The inset shows the differential df/dT of the data (points) fitted to a Gaussian (curve) centered on $T_c^{\text{Gauss}} = 9.38$ K, with a full width of $T_c^{\text{Gauss}} = 0.7$ K (after Reference [140]).

resistance between the superconducting and normal behaviour. This effect is seen over a restricted temperature range in a number of Cu-containing π -phase salts [74, 141, 142]; it is most noticeable when the current is driven in the interplane direction [141, 142]. A weaker effect can be observed when the current is driven in-plane, but is suppressed when the number of defects in the sample is reduced [143, 144]. By contrast, the "hump" is largest when the current is in the interplane direction for very pure samples [145], so that it may be an intrinsic feature of these layered materials [145]. The hump has been attributed to dissipation due to superconducting weak links in inhomogeneous samples [142], magnetoresistance due to a lattice distortion via coupling with the quantised vortices [146] and dissipation caused by fluctuations characteristic of a d-wave superconductor [147]. Note that the "hump" disappears in in-plane fields ($\theta = 90^\circ$) [148, 149], indicating that it is associated in some way with the arrangement of the vortices relative to the crystal structure [150]. This may favour the Josephson-junction model [143, 151], since this involves a noise voltage associated with thermal fluctuations

which disrupts the phases of the order parameter between adjacent Josephson-coupled planes; it will only be operative when the vortex cores traverse those planes. It has been already been established that because $-(\text{BEDT-TTF})_2\text{Cu}(\text{NCS})_2$ is a very anisotropic superconductor, the vortex lattice is no longer a system of rigid rods but consists of a weakly coupled stack of "pancake" vortices, each one confined to a superconducting plane, with the coupling due to Josephson or electromagnetic effects [104, 152] (see Section 4.3).

Whatever the mechanism, these considerations imply that the hump and the broad transition from zero to finite resistance are both phenomena of the mixed state; i.e. the dissipative effects mean that resistive measurements of the critical field are often a poor guide to reality. Figure 22(a) shows a comparison of the various techniques for deducing H_{c2} in $-(\text{BEDT-TTF})_2\text{Cu}(\text{NCS})_2$ (field applied perpendicular to the quasi-two-dimensional planes); the data comprise filled triangles (MHz penetration studies, midpoint), filled circles (microwave penetration studies), open circles (thermal conductivity data) and shaded diamonds (magnetisation data). (A number of studies have shown that GHz and MHz penetration measurements are a much less dissipative probe of the superconducting state than a resistivity measurement; see Reference [29] and references therein.) These are compared with the low-field (X , joined by dashed lines) and high-field (crosses, joined by dotted lines) limits of the resistive transition [155]. Whereas the thermal conductivity, GHz and MHz data are in good agreement with each other, following quite closely the convex curve ($T_c - T)^{2/3}$ [29], the resistive transition follows a very different concave temperature dependence, perhaps related more closely to the irreversibility line than to H_{c2} .

The phase diagrams in Figure 22(a) and (b) are completed by the inclusion of further data from SR and magnetometry studies. The triangles are the irreversibility field from magnetisation; the filled squares and stars represent two-dimensional melting from magnetometry and GHz studies. The hollow squares are from muon-spin rotation and denote the three-dimensional-two-dimensional transition.

Figure 23 shows a similar phase diagram for $-(\text{BETS})_2\text{GaCl}_4$ (conducting planes perpendicular to the applied magnetic field), determined using MHz penetration techniques [29]. $-(\text{BETS})_2\text{GaCl}_4$ is of great interest because it has a Fermi surface which is topologically similar to that of $-(\text{BEDT-TTF})_2\text{Cu}(\text{NCS})_2$, and very similar effective masses [29]. However, in contrast to $-(\text{BEDT-TTF})_2\text{Cu}(\text{NCS})_2$, which has an interlayer transfer integral $t_z = 0.04$ meV, $-(\text{BETS})_2\text{GaCl}_4$ is rather more three-dimensional, possessing an interlayer transfer integral $t_z = 0.21$ meV [29]. In $-(\text{BETS})_2\text{GaCl}_4$, H_{c2} has a linear region $H_{c2} / (T_c - T)$ that spans from T_c to approximately 1.9 K. Below 1.9 K, a definite change in the slope of the upper critical field occurs, and H_{c2} begins to follow the power law $H_{c2} / (T_c - T)^{1/2}$, with T_c and t_z parameters; powers in the range 0.5–0.7 provide an adequate fit to the data. The behaviour of H_{c2} in $-(\text{BETS})_2\text{GaCl}_4$ at temperatures below 1.9 K is therefore very similar to that of H_{c2} in $-(\text{BEDT-TTF})_2\text{Cu}(\text{NCS})_2$ over the whole temperature range shown in Figure 22, and is thus characteristic of a two-dimensional superconductor with weakly-coupled

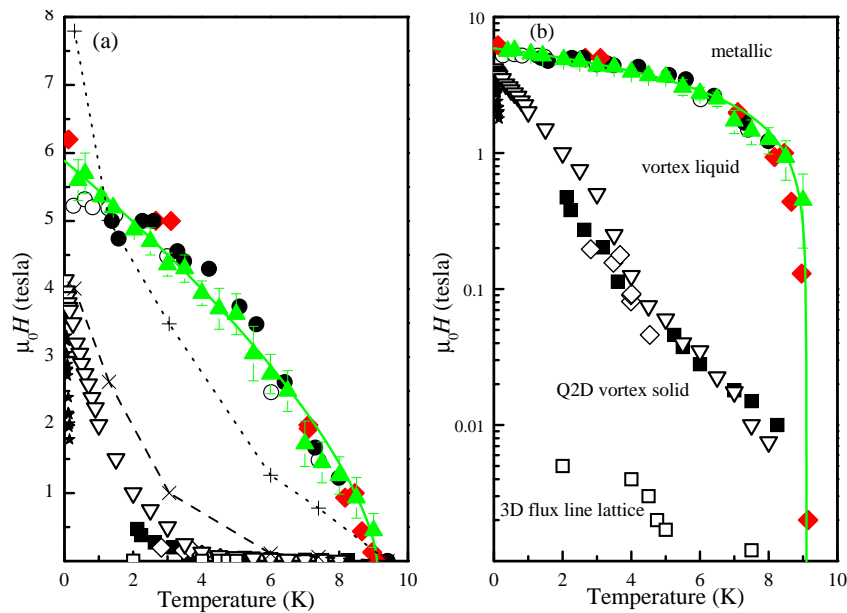


Figure 22. Critical fields in $-(\text{BEDT-TTF})_2\text{Cu}(\text{NCS})_2$, plotted on linear (a) and logarithmic (b) field scales; B is perpendicular to the quasi-two-dimensional layers. The data for H_{c2} comprise filled triangles (MHz penetration studies, midpoint) [153], filled circles (microwave penetration studies) [155], open circles (thermal conductivity data) [155] and shaded diamonds (magnetisation data) [50, 86]. The solid curve is proportional to $(T_c - T)^2=3$, with $T_c = 9.1$ K. The triangles are the irreversibility field from magnetisation; the filled squares and stars represent two dimensional melting from magnetometry and GHz studies [154] (see also Reference [96]). The hollow squares are from muon-spin rotation and denote the three dimensional-two dimensional transition [104]. (a) also shows the low-field (X , joined by dashed lines) and high-field (crosses, joined by dotted lines) limits of the resistive transition [155]. (After Reference [29].)

layers [154]. On the other hand, the linear variation of H_{c2} in $-(\text{BETS})_2\text{GaCl}_4$ at higher temperatures follows the expectations of Ginzberg-Landau theory for three-dimensional superconductors [78, 156]. The change in gradient at 1.9 K is therefore attributed to dimensional cross-over from quasi-two-dimensional (low temperatures) to three dimensional (high temperatures) [29].

Dimensional crossovers with the magnetic field applied perpendicular to the quasi-two-dimensional planes have been observed in artificial quasi-two-dimensional superconducting structures [157, 158] and in organic superconductors such as $-(\text{BEDT-TTF})_2\text{Cu}(\text{NCS})_2$ (see Figure 22) [104, 154]; however, in the majority of these cases, the effect of the crossover is observed at magnetic fields less than H_{c2} . $-(\text{BETS})_2\text{GaCl}_4$ is perhaps unique in providing the correct anisotropy for the crossover to be observed in the behaviour of $H_{c2}(T)$. It has been mentioned that the interplane transfer integral in $-(\text{BETS})_2\text{GaCl}_4$ is a factor 5 larger than that in $-(\text{BEDT-TTF})_2\text{Cu}(\text{NCS})_2$. The greater "three dimensionality" of the bandstructure of $-(\text{BETS})_2\text{GaCl}_4$ compared to $-(\text{BEDT-TTF})_2\text{Cu}(\text{NCS})_2$ obviously manifests itself in the superconducting behaviour

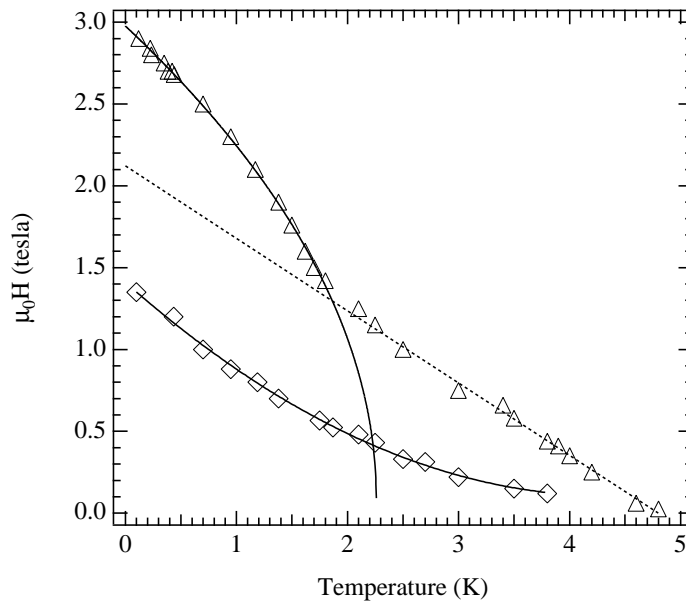


Figure 23. Critical fields in $-(\text{BEDT-TTF})_2\text{Cu}(\text{NCS})_2$ (with B perpendicular to the quasi-two-dimensional layers) measured using MHz penetration techniques. The data comprise H_{c2} (triangles) and flux-line lattice melting (diamonds). The upper solid curve is $H_{c2} / (T - T_c)^{1/2}$; the dashed curve is $H_{c2} / (T_{c2} - T)$. The lower solid curve is a fit of the two-dimensional model expression for the flux-line lattice melting. (After Reference [29].)

(compare Figures 23 and 22); whereas $-(\text{BEDT-TTF})_2\text{Cu}(\text{NCS})_2$ exhibits two dimensional-three dimensional dimensional crossover in its $H_{c2}(T)$ behaviour, $H_{c2}(T)$ in $-(\text{BEDT-TTF})_2\text{Cu}(\text{NCS})_2$ is entirely characteristic of a quasi-two-dimensional superconductor.

4.2. Anisotropy of the superconducting parameters.

A number of studies of the anisotropy of the upper critical field of $-(\text{BEDT-TTF})_2\text{Cu}(\text{NCS})_2$ have been made, all employing resistivity measurements [148, 149, 159] (for a summary, see Section 3.4 of Reference [1]). The angle-dependent behaviour of $-(\text{BEDT-TTF})_2\text{Cu}(\text{NCS})_2$ seems to be rather typical of quasi-two-dimensional organic superconductors, and as the studies of this salt are the most detailed, we shall focus on them.

As we have seen above, the resistive transition is often a poor guide to the temperature dependence of H_{c2} ; however, most of the anisotropy studies were carried out at fixed temperatures [148, 149, 159], and some attempts were made to choose a characteristic point in the resistivity which took account of the fact that the "hump" is a feature of the mixed state [8]. To the limit of experimental accuracy, it was found that H_{c2} depended only on θ , the angle between the normal to the quasi-two-dimensional planes and the magnetic field; in spite of some expectations to the contrary, it appears that H_{c2} is rather insensitive to the plane of rotation of the field [149].

For an exactly in-plane field ($\theta = 90^\circ$), H_{c2} reaches its maximum value of $\mu_0 H_{c2}(T \rightarrow 0) = 3.5 \text{ T}$ in $-(\text{BEDT-TTF})_2\text{Cu}(\text{NCS})_2$ [8]. Away from this orientation,

the variation of H_{c2} with θ is at first sight qualitatively similar to the predictions of the Ginzberg-Landau anisotropic effective mass approximation [148, 159, 78, 160],

$$B_{c2}(\theta) = \frac{B_{c2}(\theta = 0)}{\cos^2(\theta) + \gamma^2 \sin^2(\theta)}; \quad (6)$$

in which the superconductivity is destroyed by orbitale cts; here γ is the square root of the ratio of the effective masses for interplane and in-plane motion respectively. However, whilst Equation 6 has a similar form to the published data [148, 149, 159], a very serious failure of this approach becomes apparent when one compares the value $\gamma \approx 10$ obtained by fitting H_{c2} data to Equation 6 with the accepted value of $\gamma \approx 100 - 350$ obtained from very careful measurements of the penetration depths [105, 106, 109, 152]. These large values of γ occur because the coherence length perpendicular to the conducting layers, ξ_{\perp} , is smaller than the interlayer distance a . The intralayer overlap of electron wave functions in the superconducting state is very weak because ξ_{\parallel} is shorter than the Josephson tunnelling length $l_J = a/\gamma$ (γ is a constant) between Josephson vortices in $-(BEDT-TTF)_2Cu(NCS)_2$ [152]. In sufficiently high magnetic fields parallel to the layers, flux lines will be trapped inside the layers; in such a limit, the compressing effect of the magnetic field on the Cooper pair wavefunction [161] exactly compensates the increasing flux density, potentially leading to a very high in-plane upper critical field [163] if orbitale cts are the limiting mechanism. This is obviously not observed in the data of References [159, 148, 149]; some other mechanism therefore seems to be limiting the upper critical field close to $\theta = 90^\circ$.

Kovalev et al. [162] used an elegant series of heat capacity measurements to show that the in-plane $\theta = 90^\circ$ upper critical field is in fact limited by processes associated with the quasiparticle spin in π -phase BEDT-TTF salts. A possible candidate is the Pauliparamagnetic limit (PPL), also known as the Clogston-Chandrasekhar limit [164, 165, 166]. This occurs when the magnetic energy associated with the spin susceptibility in the normal state exceeds the condensation energy in the superconducting state; for isotropic s-wave superconductors it is given by

$$\mu_0 H_{PPL}(T = 0) = 1.84 T_c; \quad (7)$$

The PPL mechanism should be roughly isotropic (as the electron g-factor in organic superconductors is within a few percent of 2 for all field orientations [13]). Bulaevskii [167] considered the case where the paramagnetic limit is larger than $H_{c2}(\theta = 0)$, but smaller than $H_{c2}(\theta = 90^\circ)$ determined by orbitale cts. In a similar spirit Nam et al. proposed a semi-empirical description of the critical field representing an anisotropic orbital limiting mechanism, dominant at lower values of θ , combined with an isotropic PPL-type mechanism which limits the critical field close to $\theta = 90^\circ$ (Equation 3 of Reference [149]); in practice, with some rearrangement, this equation gives an identical angle dependence to Equation 6.

A critical comparison between the various predicted angle-dependences of H_{c2} and resistive critical field data has been made in References [148] and [149]. However, none of the formulae give a truly satisfactory fit over the whole angular range, the fits in

Reference [148] describing the data close to $\theta = 90^\circ$ but apparently failing at angles away from this orientation. By contrast, the expression used in Reference [149] only fits the data away from $\theta = 90^\circ$; data for θ close to 90° do not seem to follow the same dependence. Two proposals have been made to account for this difference. Firstly, Zuo et al. [148] argued that the paramagnetic limiting field could be calculated from thermodynamic arguments to be 30 ± 5 T, considerably larger than the value predicted by Equation 7. An alternative proposal was made in Reference [149], based on the inability of conventional formalisms to fit the angle dependence of B_{c2} close to $\theta = 90^\circ$; to explain this, and the large values of B_{c2} , the existence of a Fulde-Ferrell-Larkin-Ovchinnikov (FFLO) [168] state in high in-plane fields and at low temperatures was invoked [149]. As we shall see in Section 5.1, the latter explanation seems to be the correct one [8].

In summary, the upper critical field H_{c2} in α -phase organic superconductors is limited by orbital effects for most orientations of the field, but limited by processes involving the quasiparticle spin when the field lies in the quasi-two-dimensional planes. This implies that estimates of the interlayer coherence length derived from the in-plane critical field [13] are incorrect. A better guide to the true anisotropies of organic superconductors is derived from magnetisation [152], penetration-depth [105] and SR studies [104, 112]; such studies indicate $\lambda_{ab} \approx 350$ Å for $-(\text{BEDT-TTF})_2\text{Cu}(\text{NCS})_2$.

4.3. The vortex lattice.

The vortex lattice in BEDT-TTF superconductors has been studied by SR [104, 112] and by flux decoration techniques [169]. Both types of experiment reveal a triangular flux-line lattice at the lowest fields, with the SR data showing some evidence for a transition to a square lattice at higher fields and temperatures, just before the layers become decoupled (see Figure 24) [112].

A key question for the SR experiments is the mechanism (Josephson or electromagnetic [170]) for the interlayer coupling of the vortices. Table 1 summarises some of the recent SR data [112], comparing the experimental magnetic field B_{cr}^{meas} for the transition from flux-line lattice to decoupled layers with that calculated assuming electromagnetic coupling (B_{cr}^{EM}). The table also compares measured and calculated temperatures T_c for the thermal break up of the flux-line lattice. The comparison between the measured and calculated parameters allows the coupling mechanism to be inferred. It appears that coupling in the more anisotropic BEDT-TTF superconductors is predominantly electromagnetic in origin.

5. Field-induced superconducting states.

5.1. The Fulde-Ferrell-Larkin-Ovchinnikov phase in $-(\text{BEDT-TTF})_2\text{Cu}(\text{NCS})_2$

There has been great interest in the possibility of the Fulde-Ferrell-Larkin-Ovchinnikov (FFLO) [168] state in organic superconductors for some time [171]. In a metal in a

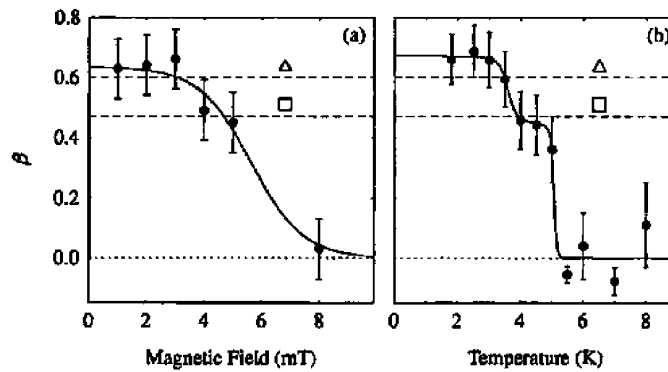


Figure 24. Skewness parameter g of $-(\text{BEDT-TTF})_2\text{Cu}(\text{NCS})_2$ plotted as a function of magnetic field at a temperature of 2 K (a) and as a function of temperature at a field of 3 mT (b). The skewness parameter, determined in SR experiments [107], takes on very characteristic values for different types of flux lattice. The crossover from three-dimensional flux-line lattice to decoupled layers is observable as the drop in g seen between 5 and 8 mT in (a). The expected ranges of g for triangular and square lattices are denoted by the square and triangle symbols and the dashed lines. There is some evidence for a triangular to square transition, especially in (b) (after Reference [112]).

Salt	η	$B_{\text{cr}}^{\text{meas}}$ (mT)	$B_{\text{cr}}^{\text{EM}}$ (mT)		mode	T_c (K)	T (K)	T_{calc} (K)
$-(\text{ET})_2\text{IBr}_2$	0.86	> 8	2.8	< 300	J	2.2	1.7	1.8
$-(\text{ET})_2\text{Cu}(\text{NCS})_2$	0.54	5.9	7.1	350	EM/J	9.2	3.9	4.5
$-(\text{ET})_2\text{NH}_4\text{Hg}(\text{SCN})_4$	1.1	1.7	1.7	> 500	EM	1.1	0.6-0.8	1.4

Table 1. Summary of recent SR data [112]. The parameters listed are the anisotropy η , the experimental magnetic field $B_{\text{cr}}^{\text{meas}}$ for the transition from flux-line lattice to decoupled layers, the corresponding calculated field assuming electromagnetic coupling ($B_{\text{cr}}^{\text{EM}}$), the superconducting transition temperature T_c and the measured and calculated temperatures T for the thermal break up of the flux-line lattice. The comparison between the measured and calculated parameters allows the coupling mode (Josephson (J) or Electromagnetic (EM)) to be inferred.

magnetic field, the normal quasiparticles have separate spin-up and spin-down Fermi surfaces which are displaced due to the Zeeman energy. In the FFLO state, attractive interactions of quasiparticles with opposite spin on opposite sides of the two Fermi surfaces lead to the formation of pairs with nonzero total momentum [168, 171] and hence an inhomogeneous superconducting state. It was suggested that the quasi-two-dimensional (quasi-two-dimensional) superconductor $-(\text{BEDT-TTF})_2\text{Cu}(\text{NCS})_2$ in exactly in-plane magnetic fields is a possible candidate for the FFLO [149, 172]; in this section, we describe recent experiments which suggest that this indeed does occur [8]. Although the FFLO phase was predicted in the mid 1960s, the experiments on $-(\text{BEDT-TTF})_2\text{Cu}(\text{NCS})_2$ seem to be the first to give definite evidence for such a state (see Reference [8] for a critique of earlier claims).

The experiments employed single crystals of $-(\text{BEDT-TTF})_2\text{Cu}(\text{NCS})_2$ ($\eta = 0.5$

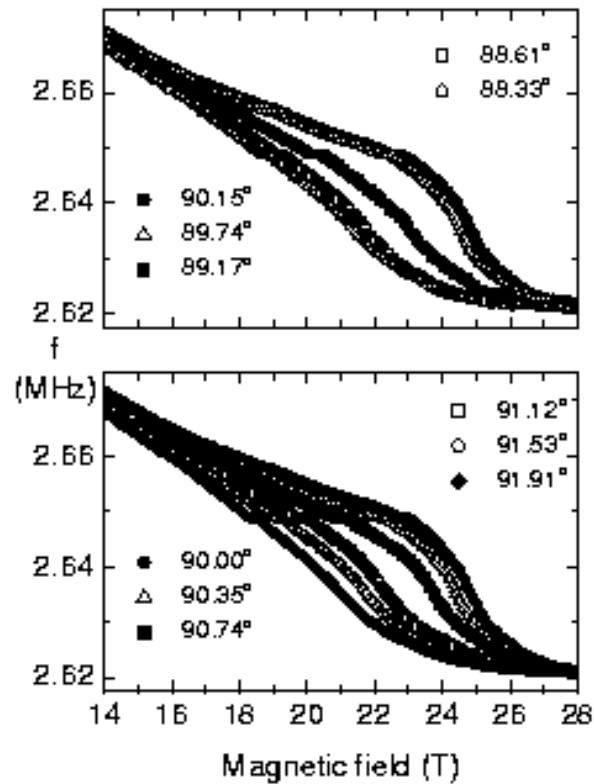


Figure 25. TCDs frequency versus magnetic field for several different values of θ ($\phi = 45^\circ$; $T = 1.39$ K). The elbow at $B_L \approx 22$ T disappears when the angle differs from 90° by more than about 1.5° (after Reference [8]).

0.1 mm^3 ; mosaic spread $< 0.1^\circ$) mounted on or in the coil of a tuned-circuit differential susceptometer (TCDs) [8]. The coil was mounted in a cryostat which allowed it (and the sample) to be rotated to all possible orientations in the magnetic field B . The orientation of the sample is defined by the polar angle θ between B and the normal to the sample's bc planes and the azimuthal angle ϕ ; $\phi = 0$ is a rotation plane of B containing b and the normal to the bc plane.

In order to detect the FFLO, Reference [8] examined the rigidity of the vortex arrangement, which is predicted to change on going from mixed state to FFLO [173]. The sample was mounted with its quasi-two-dimensional planes perpendicular to the axis of the TCDs coil. When the quasistatic field is in the sample planes ($\theta = 90^\circ$), the TCDs coil provides an oscillating magnetic field perpendicular to the static field (and the vortices) which exerts a torque on the vortices. The coil in the TCDs forms part of a tank circuit, so that changes in the rigidity of the vortices affect the effective

"stiffness" of the circuit and therefore shift its resonant frequency f .

Figure 25 shows f for several angles $\theta = 90^\circ$. Superimposed on the gentle downward trend, due to the growing flux penetration of the sample, is an "elbow" at 22 T for values of θ close to zero. The elbow indicates a change in the vortex rigidity which was associated with the onset of the FFLO state at a magnetic field labelled B_L . The elbow only occurs for $j \parallel j$ less than about 1.5; this is in good agreement with the calculations of Refs. [172, 173], which predict that the FFLO is only stable in typical organic conductors for $j \parallel j < 0.3 \div 0.3$. For bigger deviations, a substantial number of closed orbits will be possible on the Fermi surface [33], leading to suppression of the superconductivity due to orbital effects [8].

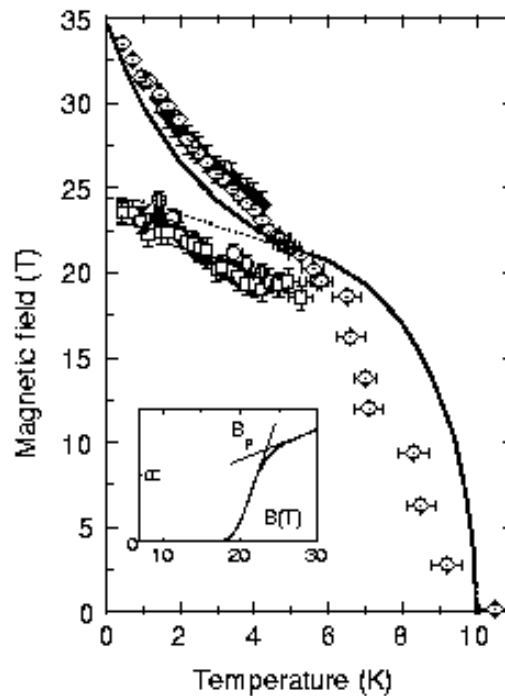


Figure 26. Temperature dependence of the fields B_L (squares, circles) and B_P (diamonds; the field B_P is defined in the inset as the intersection of the two extrapolations); the different symbols indicate data from different samples and experimental runs. The data are compared with the FFLO phase diagram of Shimahara; the solid curve separates the superconducting and normal states. The boundary between the mixed state and the FFLO is shown as a dotted line (after Reference [8]).

Figure 26 compares B_L with the calculated FFLO phase diagram of Ref. [174], derived for a quasi-two-dimensional metal; also plotted are values of the resistive upper critical field B_P ($\theta = 90^\circ$), defined in the inset to Fig. 26. The theoretical curves have been scaled using a $T = 0$ B_{c2} of 35 T and $T_c = 10$ K. Even though there are (not unexpected { see Section 4.1) deviations of B_P from the theoretical dependence of B_{c2} , the data in Fig. 26 bear a striking similarity to the calculations of Ref. [174]. In

particular, B_L follows the phase boundary between the Type-II superconducting state and the FFLO state (dotted curve) closely, extrapolating to B_p at $T = 0.56T_c$. The meeting of the two phase boundaries at $T = 0.56T_c$ is a robust feature of models of the FFLO, irrespective of dimensionality [174]. Note that the effect is very reproducible; data for different samples and different cooling and bias conditions are shown in Fig. 26; all follow the same trends [8].

In summary, when the field lies in the quasi-two-dimensional planes of $-(BEDT-TTF)_2Cu(NCS)_2$, there is good evidence for a transition into a Fulde-Ferrell-Larkin-Ovchinnikov (FFLO) state. The data are in agreement with theoretical predictions [8].

5.2. Field-induced superconductivity in $-(BETS)_2FeCl_4$

There has been considerable interest in the material $-(BETS)_2FeCl_4$, which shows a transition to what appears to be a superconducting state in an accurately in-plane magnetic field [7] (Figure 27). In this salt, the Fe^{3+} ions within the $FeCl_4$ anion molecules order antiferromagnetically at low temperatures and low magnetic fields (see Reference [7] and references therein). As is the case in most antiferromagnetic materials, the magnetic order causes $-(BETS)_2FeCl_4$ to become an insulator. On raising the magnetic field (applied exactly within the planes), the magnetic moments of the Fe^{3+} ions tilt (i.e. become "canted"), and then the long-range magnetic order is destroyed, leaving a paramagnetic metal [7]. Further increases in field induce the superconducting state at about 16 T [7].

Field-induced superconductivity in magnetic materials is usually discussed in terms of the Jaccarino-Peter compensation (JPC) effect, in which the applied field "compensates" the internal magnetic field provided by the magnetic ions (in the case of $-(BETS)_2FeCl_4$, the Fe^{3+} ions). The JPC effect was predicted in the early 1960s [175], and observed almost twenty years ago in $Eu_xSn_{1-x}Mo_6S_8$ [176].

Therefore, the situation in $-(BETS)_2FeCl_4$ seems to be as follows. The applied magnetic field compensates the internal field provided by the Fe^{3+} ions, so that superconductivity (which would otherwise be suppressed by the magnetism) can occur at fields above 16–20 T [7, 177]. The previous sections have shown that a quasi-two-dimensional superconductor can attain high upper critical fields if the magnetic field is applied exactly in the plane of the layers. In such a configuration, only a very small number of closed orbits can occur on the Fermi surface. Hence, the orbital interactions which would otherwise overwhelm the superconductivity are suppressed [149]. The magnetic field can then only destroy the superconductivity via the Zeeman effect, leading to an upper critical field determined by the Pauli limit or a more exotic mechanism such as the FFLO. It is notable that the field-induced superconductivity in $-(BETS)_2FeCl_4$ only occurs when the magnetic field is exactly within the layers.

Because of this, with the magnetic field applied exactly within the layers, $-(BETS)_2FeCl_4$, in common with other quasi-two-dimensional organic superconductors (see Sections 4.2 and 5.1), has a high upper critical field because orbital effects are

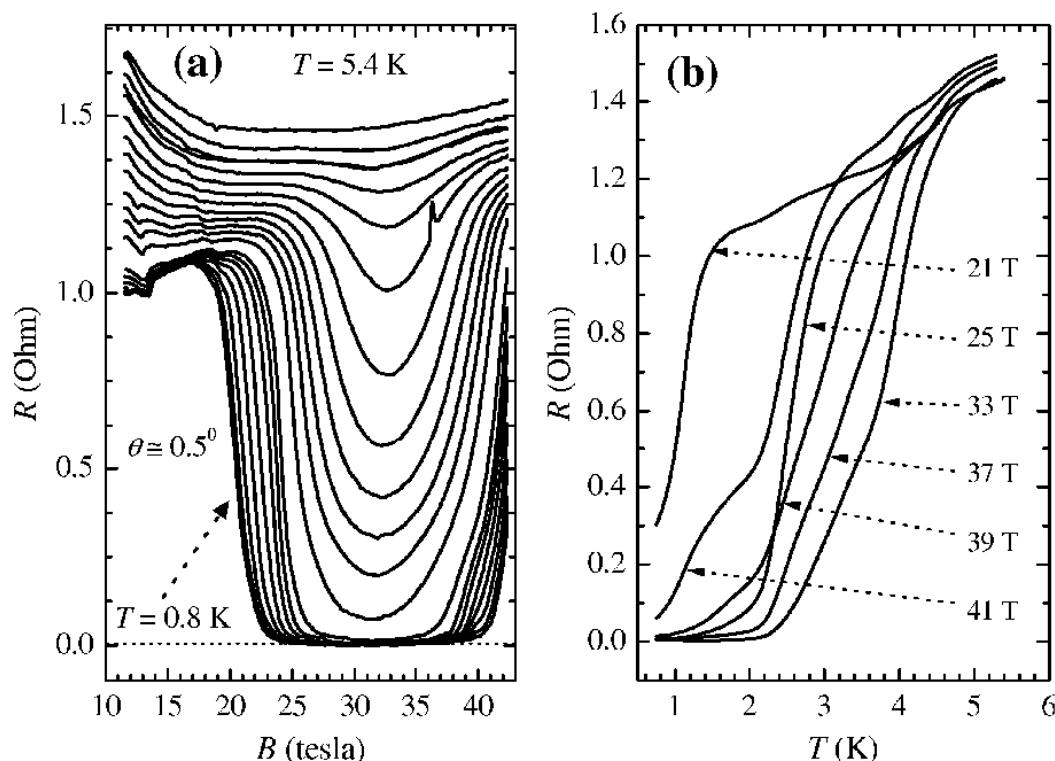


Figure 27. Resistance of a crystal of $-(\text{BETS})_2\text{FeCl}_4$ (a) as a function of magnetic field for temperatures between 800 mK and 5.4 K and (b) as a function of temperature for various magnetic fields (after Reference [177]). The magnetic field is applied within the quasi-two-dimensional planes of the crystal. Note the strong minimum in the resistance, suggestive of superconductivity.

suppressed. This allows the material to continue to superconduct to fields well above 16 T. Recent measurements [177] suggest that the upper critical field is around 40 T, the material regaining measurable resistance above this field (Figure 27).

Whilst this simple picture accounts qualitatively for most aspects of the data presented thus far, there are undoubtedly further complications, and much work remains to be done. Whereas the Cooper pairs in conventional superconductors are formed via electron-phonon interactions, there is evidence that the pairing interactions in organic superconductors involve magnetic excitations (see Section 3.1.1). The interaction between these excitations and the magnetic moments of the Fe^{3+} ions undoubtedly complicates the simple effects described above.

5.3. Persistent currents in the high-field state of $-(\text{BEDT-TTF})_2\text{KHg}(\text{SCN})_4$

Prior to the development of the BCS theory, Frohlich proposed that superconductivity would occur in quasi-one-dimensional metals due to spontaneously sliding charge-density

waves (CDW s) [178]. CDW s were subsequently discovered in many materials with quasi-one-dimensional Fermi-surface sections [179]. However, the opening of the energy gap, and pinning to impurities, generally prevent a CDW from contributing to the electrical conductivity, so that the transport properties are dominated by any remaining normal carriers [179]. Depinning of CDW s may occur under large electric fields, but is accompanied by considerable dissipation.

However, recently, Harrison et al. have made measurements that appear to support the presence of something like a superconducting state in $-(\text{BEDT-TTF})_2\text{KHg}(\text{SCN})_4$ at high magnetic fields. This may be a Frohlich superconductor, or could possibly entail a more exotic mechanism involving the dynamic exchange of quasiparticles between the density wave in the quasi-one-dimensional Fermi-surface section and a quasi-two-dimensional pocket also present [180].

In its normal state, $-(\text{BEDT-TTF})_2\text{KHg}(\text{SCN})_4$ has a Fermi surface consisting of a quasi-two-dimensional pocket and a pair of sheets, the sheets nesting at low temperatures to give the commensurate CDW₀ phase [1, 9]. The phase diagram is shown in Figure 28; at a field of 23 T, the CDW₀ phase reaches its Pauli paramagnetic limit and transforms into the incommensurate CDW_x phase, with a very low transition temperature ~ 2 K.

$-(\text{BEDT-TTF})_2\text{KHg}(\text{SCN})_4$ is therefore unusual in two respects: (1) it exhibits a CDW state in which the gap energy Δ_0 is sufficiently small for such a transition to occur in accessible magnetic fields; and (2) the reduced gap $\Delta_x \sim 1$ meV that characterizes the CDW_x phase is $\sim 10^2$ smaller than those in typical CDW materials [179].

In the Frohlich interpretation of Harrison's data, the smallness of the gap means that the zero-point energy of the CDW_x phase dramatically exceeds the pinning potential, allowing the CDW to slide freely [9]. In the alternative explanation [180], the smallness of the pinning potential is also a key factor, allowing the CDW to change its nesting vector (with some resistance) in response to the changing field. Whatever the explanation, within the CDW_x phase (see Figure 28), robust persistent currents are seen in magnetisation data, behaving in exactly the same manner as do those found in an inhomogeneous type II superconductor [9].

Interestingly, the persistent currents seen in $-(\text{BEDT-TTF})_2\text{KHg}(\text{SCN})_4$ were for some time attributed to the quantum Hall effect and its attendant chiral Fermi liquid (see Section 4.6.2 of Reference [1] and Reference [181] for a review). The CDW formation is of course due to the quasi-one-dimensional section of the Fermi surface; however, in the CDW_x phase, the density wave coexists with very sharp Landau levels of the quasi-two-dimensional Fermi surface (see inset to Figure 28). The presence of the Landau levels appears to modulate the size and nature of the persistent currents provided by the density wave [9]. It was this apparent Landau-level filling factor dependence which led to proposals of the involvement of the quantum Hall effect [9, 180].

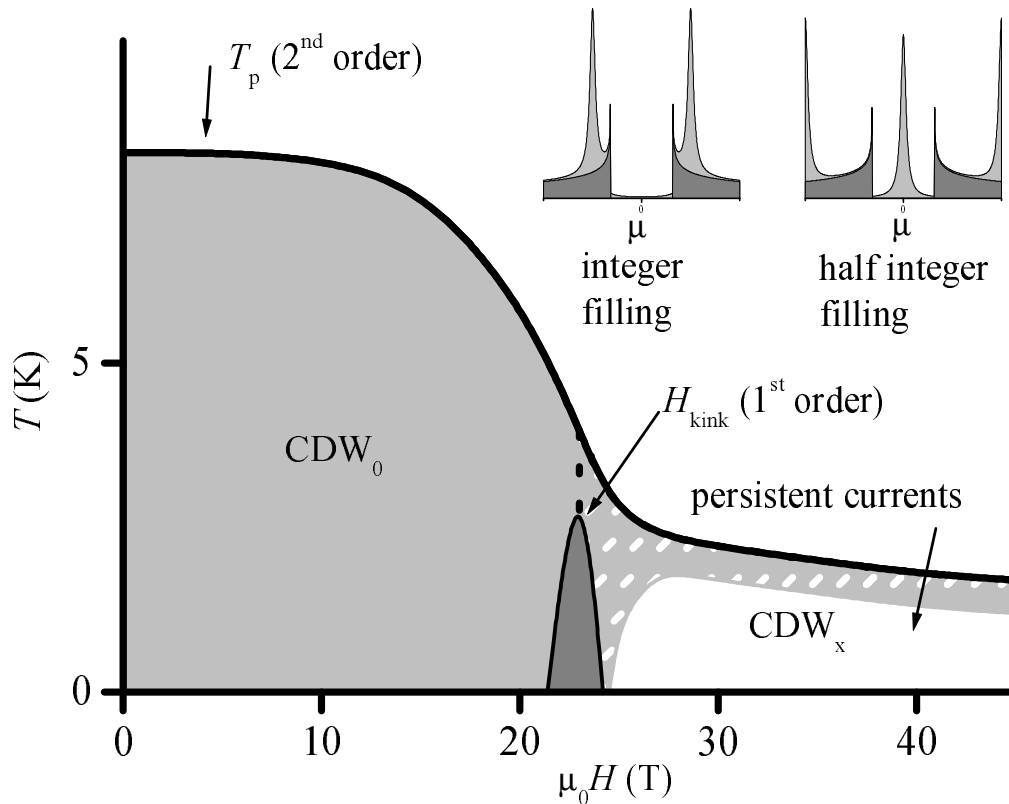


Figure 28. Notional phase diagram of $-(\text{BEDT-TTF})_2\text{KHg}(\text{SCN})_4$ constructed from theoretical models and data (see Reference [9]). The solid line represents a second order transition into the CDW phase (light shading) with a dotted line [together with the region of hysteresis (heavy shading)] representing a first order transition between the proposed CDW₀ (solid shading) and CDW_x (hatched shading) phases. Persistent currents (white region) are observed only within the CDW_x phase. The top right-hand corner shows the density of states resulting from CDW formation within the 1D bands (heavy shading) together with the contributions from the Landau levels of the two dimensional band (light shading), both at integer and half integer filling factors. μ represents the position of the chemical potential.

6. Summary

It is hoped that this review has outlined some of the many reasons for studying quasi-two-dimensional organic superconductors. These systems form a unique "test-bed" for ideas about the superconducting state; in contrast to many other types of superconductor, their (usually simple) Fermi surfaces may be readily measured to great accuracy. Subsequently "chemical" or real pressure can be used to vary the bandstructure controllably, and the consequent changes in superconducting properties studied.

In spite of the strong interactions, a Fermi-liquid approach seems at present able

to describe the properties of the normal-state quasiparticles (see e.g. [66]), although intensive searches continue for departures from this conforming behaviour. However, much work remains to be done on the question of the interactions involved in the superconductivity. Although it is clear that electron-phonon and electron-electron interactions, and antiferromagnetic fluctuations all play a part in the superconducting mechanism, their exact role is yet to be determined. Questions such as this, plus the emergence of new organic superconductors with even more exotic phase diagrams [182] will ensure that this field remains a very active one for some time to come.

7. Acknowledgements

Work on organic conductors at Los Alamos is supported by the Department of Energy, the National Science Foundation (NSF) and the State of Florida, and that at Oxford is supported by EPSRC (UK). We should like to thank Albert Migliori, Paul G. Oddard, Arzhang Ardavan, Anne-Katrin Kohn, Francis Pratt, Stan Tozer, Neil Harrison, Bill Hayes, Francis Pratt, Jim Brooks, Joerg Schmalian, Luis Balicas, Phil Anderson and Steve Blundell for useful discussions and encouragement. Part of this article was written at the Aspen Center for Physics; JS expresses his gratitude for the opportunity to work in such a stimulating environment.

8. Note added in proof

Further strong evidence for d-wave superconductivity in α -phase BEDT-TTF salts comes from very recent thermal conductivity experiments; see K. Izawa, H. Yamaguchi, T. Sasaki and Y. Matsuda, *Phys. Rev. Lett.* 88, 027002 (2002).

9. Biographical details

After a doctorate in semiconductor physics, and a postdoctoral research fellowship at Oxford University, John Singleton worked at the High Field Magnet Laboratory, Katholieke Universiteit Nijmegen. It was in Nijmegen, on the advice of Bill Hayes and Francis Pratt (Oxford), that he began to study organic superconductors using high magnetic fields. In 1990, John returned to Oxford University as a Lecturer in Physics (since promoted to Reader in Physics). Since then he has helped to establish the Oxford Correlated Electron Systems Group, a collection of about twenty academics, postdocs, students and visitors working on organic metals and magnets, electrically-conductive metal oxides, heavy-fermion compounds, small biological molecules and novel solid-state light sources. He spent the academic year 2000-2001 as a visiting scientist at the National High Magnetic Field Laboratory, Los Alamos.

Charles (Chuck) Melike received his doctorate (on various organic conductors) from Clark University, Worcester, Massachusetts, where he also helped to set up the pulsed-field magnet facility. Whilst at Clark, Chuck played a pivotal role in developing

10. R e f e r e n c e s

- [1] J. Singleton, Rep. Progr. Phys. 63, 1111 (2000).
- [2] R.M. McKenzie Comment. Cond. Mat. Phys. 18, 309 (1998).
- [3] H. Kanoda, Physica C 282, 299 (1997); Hyperf. Int., 104, 235 (1997).
- [4] K. Kuroki and H. Aoki, Phys. Rev. B 60, 3060 (1999).
- [5] J. Schmalian, Phys. Rev. Lett. 81, 4232 (1998).
- [6] Fermi surfaces of low-dimensional organic metals and superconductors by J. Wosnitza (Springer-Verlag, Berlin 1996).
- [7] S.Ujiet al., Nature 410, 908 (2001).
- [8] J. Singleton, J.A. Symington, M.S.Nam, A.Ardavan, M.Kumoo and P.Day, J.Phys.: Condens Matter 12 L641 (2000).
- [9] N.Harrison, C.H.Mielke, J.Singleton, J.S.Brooks and M.Tokumoto, J.Phys.: Condens.Matter 13, L389 (2001).
- [10] C.Bourbonnais and D.Jerome, Science 281, 1155 (1998); D.Jerome and H.J.Schulz, Adv. Phys. 31, 299 (1982); D.Jerome, Sol.State Commun. 92, 89 (1994); V.Vescoli, L.Degiori, W.Henderson G.Gruner, K.P.Starkey and L.K.Montgomery, Science 281, 1181 (1998).
- [11] J.H.Schon, Ch.Kloc, R.C.Haddon and B.Batlogg, Science 288, 656 (2000); J.H.Schon, Ch.Kloc, H.Y.Hwang, and B.Batlogg, Science 292, 252 (2000).
- [12] Mori has summarised the structural properties of virtually all organic superconductors in three excellent review articles: T.Mori, Bull.Chem.Soc.Jpn. 71, 2509 (1998); T.Mori, H.Mori, S.Tanaka, Bull.Chem.Soc.Jpn. 72, 179 (1999); T.Mori, Bull.Chem.Soc.Jpn. 72 2011 (1999).
- [13] Organic Superconductors by T.Ishiguo, K.Yamaji and G.Saito (Springer-Verlag, Berlin 1998)
- [14] L.K.Montgomery, in Organic conductors, fundamentals and applications, edited by J-P.Farges (Dekker, New York 1994), Chapter 4.
- [15] C.Proust, A.Audouard, V.Laukhin, L.Brossard, M.Honold, M.S.Nam, E.Haanappel, J.Singleton and N.Kushch, Eur.Phys.J.B 21, 31 (2001).
- [16] Band theory and electronic properties of solids, J. Singleton (Oxford University Press, Oxford, 2001).
- [17] H.Urayama, H.Yamochi, G.Saito, S.Sato, A.Kawamoto, J.Tanaka, H.Mori, Y.Manuyama, H.Inokuchi, Chem.Lett. 1988, 463 (1988).
- [18] H.Kuroda, K.Yakushi, H.Tajima, A.Ugawa, Y.Okawa, A.Kobayashi, G.Saito, Synth.Met., 27, A491 (1988).
- [19] Data extracted from tabulations and references in Section 5.2.6 of Reference [13].
- [20] J.M.Cauleld, W.Lubczynski, F.L.Pratt, J.Singleton, D.Y.K.Ko, W.Hayes, M.Kumoo and P.Day, J.Phys.: Condens.Matter 6, 2911 (1994).
- [21] John Singleton, P.A.Goddard, A.Ardavan, N.Harrison, S.J.Blundell, J.A.Schluter and A.M.Kini, preprint cond-mat 0104570, Phys.Rev.Lett. 88, 037001 (2002).
- [22] M.V.Kartsovnik, V.N.Laukhin, S.I.Pesotskii, I.F.Schegolev, V.M.Yakovenko, J.Phys.I (Paris) 2, 89 (1990).
- [23] For a more detailed discussion of the band formation in $\text{-(BEDT-TTF)}_2\text{Cu(NCS)}_2$, see Section 5.1.3 of Reference [13], Section 3.2 of Reference [1] or Reference [5] and references therein.
- [24] N.W.Ashcroft and N.D.Mermin, Solid State Physics, Saunders (1976); J.Singleton, Band theory and electronic properties of materials, Oxford University Press (2001).

- [25] N. Harrison, E. Rzepniewski, J. Singleton, P. J. Gee, M. M. Honold, P. Day and M. Kumoo, *J. Phys.: Condens. Matter* **11**, 7227 (1999).
- [26] D. Beckmann, S. Wanka, J. Wosnitza, J. A. Schlueter, J. M. Williams, P. G. Nixon, R. W. Winter, G. L. Gard, J. Ren and M. H. Whangbo, *Eur. Phys. J. B* **1**, 295 (1998); J. Wosnitza, S. Wanka, J. S. Qualls, J. S. Brooks, C. H. Mielke, N. Harrison, J. A. Schlueter, J. M. Williams, P. G. Nixon, R. W. Winter and G. L. Gard, *Synth. Met.* **103**, 2000 (1999); F. Zuo, X. Su, P. Zhang, J. S. Brooks, J. Wosnitza, J. A. Schlueter, J. M. Williams, P. G. Nixon, R. W. Winter, G. L. Gard, *Phys. Rev. B* **60**, 6296 (1999); J. Wosnitza, *Physica B* **246–247**, 104 (1998).
- [27] M. D. Oporto, J. Singleton, F. L. Pratt, J. Caulfeld, W. Hayes, J. A. J. Perenboom, I. Deckers, G. Pitsi, M. Kumoo and P. Day, *Phys. Rev. B*, **49**, 3934 (1994).
- [28] A. A. House, N. Harrison, S. J. Blundell, I. Deckers, J. Singleton, F. Herlach, W. Hayes, J. A. J. Perenboom, M. Kumoo and P. Day, *Phys. Rev. B* **53**, 9127 (1996).
- [29] Charles Mielke, John Singleton, Moon-Sun Nam, Neil Harrison, C. C. Agosta, B. Fravel and L. K. Montgomery, preprint cond-mat/0103501, *J. Phys.: Condens. Matter*, **13**, 8325 (2001).
- [30] E. Demiralp and W. A. Goddard III, *Phys. Rev. B*, **56**, 11907 (1997).
- [31] J. M. Schram, J. Singleton, R. S. Edwards, A. Ardavan, E. Rzepniewski, R. Harris, P. Goy, M. Gross, J. Schlueter, M. Kumoo and P. Day, *J. Phys.: Condens.* **13**, 2235 (2001).
- [32] M. S. Nam, S. J. Blundell, A. Ardavan, J. A. Symington and J. Singleton, *J. Phys.: Condens. Matter* **13**, 2271 (2001).
- [33] S. J. Blundell and J. Singleton, *J. Physique I* **6**, 1837 (1996).
- [34] Magnetic oscillations in metals D. Shoenberg, (Cambridge University Press, 1984).
- [35] J. Symington, P. A. Goddard, J. Singleton et al., *Synth. Met.*, in press.
- [36] M. Bird, A. Ardavan, H. Schneider-Muntau, J. Müller, National High Magnetic Field Laboratory Reports, **8** (2), 7 (2001).
- [37] T. Sasaki, H. Sato and N. Toyota, *Physics C* **185–189**, 2687 (1991); T. Sasaki, H. Sato and N. Toyota, *Solid State Commun.* **76**, 507 (1990).
- [38] N. Harrison, J. Caulfeld, J. Singleton, P. H. P. Reinders, F. Herlach, W. Hayes, M. Kumoo and P. Day, *J. Phys.: Condens. Matter* **8**, 5415 (1996).
- [39] L. B. Ioffe and A. J. Millis, *Science* **285**, 1241 (2000).
- [40] D. G. Clarke and S. P. Strong, *Adv. Phys.* **46**, 545 (1997).
- [41] C. Bergemann et al., *Phys. Rev. Lett.* **84**, 2662 (2000).
- [42] C. N. R. Rao *J. Mater. Chem.* **9**, 1 (1999).
- [43] R. H. McKenzie and P. Moses, *Phys. Rev. Lett.* **81**, 4492 (1998); *Phys. Rev. B* **60**, 11241 (1999).
- [44] This is roughly equivalent to the Mott-Ioffe-Regel criterion [45]; see e.g. [43] or Section 7.2 of [40].
- [45] N. F. Mott and E. H. Davies *Electronic properties of non-crystalline materials* (Taylor and Francis, London, 1975); A. F. Ioffe and A. R. Regel, *Prog. Semicond.*, **4**, 237 (1960).
- [46] See e.g. The theory of superconductivity in the high T_c cuprates, P. W. Anderson (Princeton University Press, 1997), page 50.
- [47] R. Louati, S. Char-Kaddour, A. Ben Ali, R. Bennaceau and M. Heritier, *Synth. Met.* **103**, 1857 (1999).
- [48] The existence of such a modulation might suggest that a beating between "neck and belly" frequencies would be observed in the dHvA effect [1]; however, in careful low-field studies [50], no such beating has been observed. We shall see that this is because the typical cyclotron energy is rather greater than t_z , even at the lowest fields used.
- [49] When viewed in the extended zone scheme, this type of Fermi surface is often known as a "coke-bottle" Fermi surface (USA) or a "Cumberland sausage" Fermi surface (Europe). (The latter is a hand-made sausage with weak but approximately regular corrugations.)
- [50] T. Sasaki, W. Biberacher, K. Neumaier, W. Hehn, K. Andres and T. Fukase, *Phys. Rev. B* **57**, 10889 (1998).
- [51] T. Otsada et al., *Phys. Rev. Lett.* **77**, 5261 (1996); N. Hanasaki et al., *Phys. Rev. B* **57**, 1336 (1998); *ibid.* **60**, 11210 (1999).

- [52] V.G. Peschansky and M.V. Kartsovnik, Phys. Rev. B 60, 11207 (1999); I.J. Lee and M.J. Naughton, Phys. Rev. B 57, 7423 (1998).
- [53] M.S. Nam et al., J. Phys.: Condens. Matter 13, 2271 (2001).
- [54] E. Ohmichi, H. Ito, T. Ishiguro, T. Komatsu and G. Saito, J. Phys. Soc. Jpn. 66, 310 (1997)
- [55] J. Wosnitza, S. Wanka et al., preprint.
- [56] J. Symington, J. Singleton, P. Goddard et al., preprint.
- [57] J. Singleton, F.L. Pratt, M. D'Amore, W. Hayes, T.J.B.M. Janssen, J.A.A.J. Perenboom, M. Kummoo and P. Day, Phys. Rev. Lett. 68, 2500 (1992).
- [58] N. Toyota, E.W. Fenton, T. Sasaki and M. Tachiki, Solid State Commun. 72, 859 (1989).
- [59] J.C.R. Faulhaber, D.Y.K. Ko and P.R. Briddon, Synth. Met. 60, 227 (1993); R.M. Vasova, S.Ya. Prievidin, V.N. Semkin, R.N. Lyubovskaya, E.I. Zhilyaeva, E.B. Yagubskii and V.M. Yartsev, Synth. Met. 48 129 (1992).
- [60] K.F. Quader, K.S. Bedell and G.E. Brown, Phys. Rev. B 36, 156 (1987); A.J. Leggett, Annals of Physics 46, 76 (1968).
- [61] Note that the cyclotron resonance data cited in Reference [20] are probably erroneous [1].
- [62] S.Hill, J. Singleton, F.L. Pratt, M. D'Amore, W. Hayes, T.J.B.M. Janssen, J.A.A.J. Perenboom, M. Kummoo and P. Day, Synthetic Metals, 55-57, 2566 (1993); S.Hill, J. Singleton, J. van Bentum, A. Wittlin, W. Hayes, M. Kummoo and P. Day, Synthetic Metals 70, 821 (1995); A. Ardavan, A. Polisskii, J. Singleton, P. Goy, M. Kummoo and P. Day, Synthetic Metals, 85, 1501 (1997); H. Ohta, Y. Yamamoto, K. Akioka, M. Motokawa, T. Sasaki and T. Fukase Synthetic Metals, 86, 2011 (1997); H. Ohta, Y. Yamamoto, K. Akioka, M. Motokawa and K. Kanoda, Synthetic Metals, 86, 1913 (1997); A. Polisski, J. Singleton and N.D. Kushch, Synthetic Metals, 86, 2197 (1997); S.Hill, J.S. Brooks, J.S. Qualls, T. Burgin, B. Fravel, L.K. Montgomery, J. Sarrao and Z. Fisk, Physica B, 246-247, 110 (1998).
- [63] A. Ardavan, J.M. Schram, S.J. Blundell, J. Singleton, W. Hayes, M. Kummoo, P. Day and P. Goy, Phys. Rev. Lett 81, 713 (1998).
- [64] A. Polisski, J. Singleton, P. Goy, W. Hayes, M. Kummoo and P. Day, J. Phys.: CM 8, L195 (1996).
- [65] S.Hill, J.S. Brooks, J.S. Qualls, T. Burgin, B. Fravel, L.K. Montgomery, J. Sarrao and Z. Fisk, Physica B 246-247, 110 (1998); S.Hill, Phys. Rev. B 55, 4931 (1997)
- [66] M.-S. Nam, A. Ardavan, J.A. Symington, J. Singleton, N. Harrison, C.H. Mielke, J.A. Schlueter, R.W. Winter and G.L. Gard, Phys. Rev. Lett., in press.
- [67] M. D'Amore, F.L. Pratt, J. Singleton, M. Kummoo and W. Hayes, Phys. Rev. Lett., 69, 991 (1992).
- [68] D. Beckmann, S. Wanka, J. Wosnitza, J.A. Schlueter, J.M. Williams, P.G. Nixon, R.W. Winter, G.L. Gard, J. Ren and M.H. Whangbo, Eur. Phys. J. B 1, 295 (1998); J. Wosnitza, S. Wanka, J.S. Qualls, J.S. Brooks, C.H. Mielke, N. Harrison, J.A. Schlueter, J.M. Williams, P.G. Nixon, R.W. Winter and G.L. Gard, Synth. Met. 103, 2000 (1999); F. Zuo, X. Su, P. Zhang, J.S. Brooks, J. Wosnitza, J.A. Schlueter, J.M. Williams, P.G. Nixon, R.W. Winter, G.L. Gard, Phys. Rev. B 60, 6296 (1999); J. Wosnitza, Physica B 246-247, 104 (1998).
- [69] K. Kanki and K. Yamada, J. Phys. Soc. Jpn. 66, 1103 (1997).
- [70] W. Kohn, Phys. Rev. 123, 1242 (1961).
- [71] J. Caulfield, W. Lubczynski, W. Lee, J. Singleton, F.L. Pratt, W. Hayes, M. Kummoo and P. Day, Synthetic Metals, 70, 815 (1995).
- [72] H. Weiss, M.V. Kartsovnik, W. Biberacher, E. Steep, A.G.M. Janssen and N.D. Kushch, JETP Lett. 66, 202 (1997).
- [73] H. Weiss, M.V. Kartsovnik, W. Biberacher, E. Steep, E. Balthes, A.G.M. Jansen, K. Andres and N.D. Kushch, Phys. Rev. B 59, 12370 (1999).
- [74] C.H. Mielke, N. Harrison, D.G. Rickel, A.H. Lacerda, R.M. Vestal and L.K. Montgomery, Phys. Rev. B 56, R4309 (1997).
- [75] M.V. Kartsovnik, W. Biberacher, K. Andres and N.D. Kushch, JETP Lett. 62, 905 (1995).
- [76] E. Ohmichi, H. Ito, T. Ishiguro, G. Saito and T. Komatsu, Phys. Rev. B 57, 7481 (1998).
- [77] A. K. Klehe, R.D. McDonald, A.F. Goncharov, V.V. Struzhkin, H.-K. Mao, R.J. Hemley, T. Sasaki,

- B 63, 104518 (2001).
- [101] K. Kuroki, T. Kikunaga, R. Arita, Y. Tanaka and Y. Matsuda, preprint cond-mat 0108506 (2001).
 - [102] J.M. Schramm, E. Rzepniewski, R. Edwards, J. Singleton, A. Ardavan, M. Kumoo and P. Day, Phys. Rev. Lett., 83, 3041 (1999).
 - [103] S. Hill, N. Harrison, M. Mola and J. Wosnitzer, Phys. Rev. Lett. 86, 3451 (2001); T. Shibauchi, Y. Matsuda, M. Baigullin, T. Tamagai, Phys. Rev. Lett. 86, 3452 (2001).
 - [104] S.L. Lee, F.L. Pratt, S.J. Blundell, C.M. Aegerter, P.A. Pattenden, K.H. Chow, E.M. Forgan, T. Sasaki, W. Hayes and H. Keller, Phys. Rev. Lett. 79, 1563 (1997).
 - [105] A. Carrington, I.J. Bonalde, R. Prozorov, R.W. Gianetta, A.M. Kini, J. Schlueter, H.H. Wang, U. Geiser and J.M. Williams, Phys. Rev. Lett., 83, 4172 (1999).
 - [106] Y. Tsubokura, M. Miyamoto, K. Ikeda, T. Nakamura and T. Takahashi, Synth. Metals 70, 913 (1995).
 - [107] For an introduction to SR, see S.J. Blundell, Contemporary Physics (1999).
 - [108] M. Pinteric, S. Tomic, M. Prester, D. Dobrac, O. Milat, K. Maki, D. Schweitzer, I. Heinen and W. Stunz, Phys. Rev. B 61, 7033 (2000).
 - [109] T. Shibauchi, M. Sato, A. Mashio, T. Tamagai, H. Mori, S. Tajima and S. Tanaka, Phys. Rev. B 55, R11977 (1997).
 - [110] Stephan Friemel, Thesis, Universite Paris XI, Orsay (1997).
 - [111] S. Belin, K. Behnia and Andre Deluzet, Phys. Rev. Lett. 81, 4728 (1998).
 - [112] F.L. Pratt, S.L. Lee, C.M. Aegerter, C. Ager, S.H. Lloyd, S.J. Blundell, F.Y. Ogrin, E.M. Forgan, H. Keller, W. Hayes, T. Sasaki, N. Toyota and S. Endo, Synth. Met. 120, 1015 (2001); F.L. Pratt et al., preprint.
 - [113] X. Su, F. Zuo, J.A. Schlueter, A.M. Kini, and J.M. Williams, Phys. Rev. B 57, R14056 (1998); Phys. Rev. B 58, R2944 (1998).
 - [114] J.M. Schramm and J. Singleton, Phys. Rev. Lett. 63, 3453 (2001).
 - [115] K. Maki, preprint.
 - [116] S. Charf-Kaddour, A. Ben Ali, M. Heritier and R. Bennaceur, J. Superconductivity 14, 317 (2001).
 - [117] J.A. Schlueter, A.M. Kini, B.H. Ward, U. Geiser, H.H. Wang, J. Mochasham, R.W. Winter and G.L. Gard, Physica C 351, 261 (2001).
 - [118] J. Muller, M. Lang, F. Steglich, J.A. Schlueter, A.M. Kini, U. Geiser, J. Mochasham, R.W. Winter, G.L. Gard, Phys. Rev. B 61, 11739 (2000).
 - [119] M.J. Rice, Phys. Rev. Lett. 37 36 (1976).
 - [120] O.O. Rozdova et al., Synth. Met. 64 17 (1994).
 - [121] S. Mazumdar and S.N. Dixit, Phys. Rev. B 34, 3683 (1986).
 - [122] M.J. Rozenberg et al., Phys. Rev. B 54 8452 (1996).
 - [123] N.L. Wang, B.P. Clayman, H. Mori and S. Tanaka, J. Phys.: Condens. Matter, 12, 2867 (2000).
 - [124] J.E. Eldridge, Y. Lin, H.H. Wang, J.M. Williams and A.M. Kini, Phys. Rev. B 57, 597 (1998).
 - [125] Y. Lin, J.E. Eldridge, H.H. Wang, A.M. Kini, M.E. Kelly, J.M. Williams and J. Schlueter, Phys. Rev. B 58, R599 (1998).
 - [126] Y. Lin, J.E. Eldridge, J. Schlueter, H.H. Wang and A.M. Kini, Phys. Rev. B 64, 024506 (2001).
 - [127] R.M. Vlasova, O.O. Rozdova, V.N. Semkin, N.D. Kusch and E.B. Yagubskii, Phys. Solid State 38 481 (1996).
 - [128] G. Vignani, A. Painelli, A. Giraldo and A. Fortunelli, Europhys. Lett. 42, 467 (1998).
 - [129] M. Dressel, J.E. Eldridge, H.M. Williams and H.H. Wang, Physica C 203 247 (1992).
 - [130] R.D. McDonald, A.K. Khe, A.P. Jephcoat, H. Olijnyk, T. Sasaki, W. Hayes, J. Singleton, J. Phys.: Condens. Matter 13, L291 (2001).
 - [131] R.D. McDonald, A.K. Khe, W. Hayes and J. Singleton, preprint cond-mat 0105316 (2001)
 - [132] G. Vignani, M. Masino, C. Bellitto and A. Giraldo, Phys. Rev. B 58, 9460 (1998).
 - [133] D. Pedron, G. Vignani, R. Bozio, J.M. Williams and J.A. Schlueter, Physica C 276, 1 (1997).
 - [134] Y. Tsubokura, T. Nakamura, T. Takahashi, L. Ikeda, Y. Nishio, K. Kajita, B. Hilti and J.S.

- Zambounis, *Synth. Metals* 85, 1515 (1997).
- [135] Y. Kobayashi, T. Nakamura, T. Takahashi, K. Kanoda, B. Hilti and J.S. Zambounis, *Synth. Metals* 70, 871 (1995).
- [136] F. Creuzet, C. Bourbonnais, G. Creuzet, D. Jerome, D. Schweitzer, H.J. Keller, *Physica B* 143, 363 (1986).
- [137] A. Nowack, U. Poppe, M. Weger, D. Schweitzer, H. Schwenk, *Z. Phys. B* 68, 41 (1987).
- [138] A. Giraldo, M. Masino, G. Visentini, R. Guido Della Valle, A. Brillante and E. Venuti, *Phys. Rev. B* 62, 14476 (2000).
- [139] B. Rothamel, L. Forro, J.R. Cooper, J.S. Schilling, M. Weger, P. Belle, H. Brunner, D. Schweitzer, H.J. Keller, *Phys. Rev. B* 34, 704 (1986).
- [140] J. Singleton, N. Harrison, C.H.M.ielke, J. Schlueter and A.M. Kini, *J. Phys.: Condens. Matter*, 13, L899 (2001).
- [141] F.L. Pratt, J. Caulfield, L. Cowey, J. Singleton, M. D'Amore, W. Hayes, J.A.A.J. Perenboom, M. Kurooo and P. Day, *Synthetic Metals*, 56, 2289 (1993).
- [142] H. Ito, T. Ishiguro, T. Komatsu, G. Saito and H. Anzai, *Physica B* 201, 470 (1994) and references therein.
- [143] T. Ishiguro, H. Ito, Yu.V. Sushko, A. Otsuka and G. Saito, *Physica B* 197, 563 (1994).
- [144] This observation might represent mixing of the interplane component of the resistivity ρ_{zz} with the in-plane components ρ_{xx} and ρ_{xy} , which will be most severe in samples with large concentrations of defects [84]; i.e. the "hump" is actually only truly present in ρ_{zz} , and the experimental measurements of the in-plane resistance in the less pure samples include a greater proportion of ρ_{zz} .
- [145] F. Zuo, X. Su, P. Zhang, J.A. Schlueter, M.E. Kelly and J.M. Williams, *Phys. Rev. B* 57 R5610 (1998).
- [146] F. Zuo, J.A. Schlueter, M.E. Kelly and J.M. Williams, *Phys. Rev. B* 54, 11973 (1996).
- [147] Kazumichi, E. Puchkaryov and Hyekyung Wong, *Synthetic Metals* 103, 1933 (1999).
- [148] F. Zuo, J.S. Brooks, R.H.M. McKenzie, J.A. Schlueter and J.M. Williams, *Phys. Rev. B* 61 750 (2000).
- [149] M.-S. Nam, J.A. Symington, J. Singleton, S.J. Blundell, A. Ardavan, J.A.A.J. Perenboom, M. Kurooo, and P. Day, *J. Phys.: Condens. Matter*, 11, L477 (1999).
- [150] Under certain conditions, dissipative mechanisms associated with vortices can also lead to a hump in the angle-dependent resistivity at $\theta = 90^\circ$; see M. Chaparala et al, *Phys. Rev. B* 53, 5818 (1996).
- [151] V. Ambegaokar and B.I. Halperin, *Phys. Rev. Lett.* 22, 1364 (1969).
- [152] P.A. Minsky, P.M. Chaikin, and R.C. Haddon, *Phys. Rev. B* 50, 15929 (1994).
- [153] J. Singleton and C.H.M.ielke, to be published (2001).
- [154] M. Mola, S. Hill, J.S. Brooks and J.S. Qualls, *Phys. Rev. Lett.* 86, 2130 (2001).
- [155] S. Belin, T. Shibauchi, K. Behnia and T. Tamagai, *J. of Superconductivity*, 12, 497 (1999).
- [156] *Superconductivity*, edited by R.D. Parks (Marcel Dekker, New York, 1969).
- [157] W.R. White, A. Kapitulnik and M.R. Beasley, *Phys. Rev. Lett.* 66, 2826 (1991).
- [158] The majority of dimensional crossover studies employing artificial layered structures focus on the effect of an in-plane magnetic field, which is not relevant in the current context; see e.g. S.T. Ruggiero, T.W. Barbee and M.R. Beasley, *Phys. Rev. Lett.* 45, 1299 (1980) and references therein.
- [159] T. Nakamura, T. Komatsu, G. Saito, T. Otsada, S. Kagoshima, N. Miura, K. Kato, Y. Manuyama and K. Oshima, *J. Phys. Soc. Jpn.*, 62 4373 (1993).
- [160] R.C. Morris, R.V. Coleman, and R. Bhandari, *Phys. Rev. B* 5, 895 (1972).
- [161] N. Dupuis and G. Montambaux, *Phys. Rev. Lett.* 68, 357 (1992); N. Dupuis and G. Montambaux, *Phys. Rev. B* 46 9603 (1992).
- [162] A.E. Kovalev, T. Ishiguro, T. Kondo and G. Saito, *Phys. Rev. B* 62, 103 (2000).
- [163] Taking the value of $\mu_0 H_{c2} = 100 - 360$ from Reference [152], the estimated in-plane critical field if

orbital effects were the only limiting factor would be $B_{c2}(\theta = 90^\circ) = B_{c2}(\theta = 0^\circ) \approx 500$ T at 1.45 K! This is plainly far higher than the experimental value.

- [164] A. M. Clogston, Phys. Rev. Lett. 9, 266 (1962).
- [165] A. M. Clogston, A. C. Gossard, V. Jaccarino, and Y. Yafet, Phys. Rev. Lett. 9, 262 (1962); K. Maki and T. Tsuneto, Progress of Theoretical Physics 31, 945 (1964).
- [166] B. S. Chandrasekhar, Phys. Rev. Lett. 1, 7 (1962).
- [167] L. N. Bulaeviskii, Int. J. Mod. Phys. B 4, 1849 (1990).
- [168] P. Fulde and R. A. Ferrell, Phys. Rev. 135 (1964) A550; A. I. Larkin and Yu. N. Ovchinnikov, Zh. Eksp. Teor. Fiz. 47 (1964) 1136; Sov. Phys. JETP 20 (1965) 762.
- [169] L. Ya. Vinnikov, T. L. Barkov, M. V. Kartsovnik, N. D. Kushch, Phys. Rev. B 61, 14358 (2000).
- [170] J. R. Clem, Phys. Rev. B 43, 2349 (1988).
- [171] H. Shimahara, J. Phys. Soc. Jpn. 66 (1997) 541; H. Shimahara, J. Phys. Soc. Jpn. 67 (1998) 1872; A. I. Buzdin and V. V. Tugushev, Zh. Eksp. Teor. Fiz. 85 (1983) 735 (Sov. Phys. JETP 85 (1983) 428); A. G. Lebed, Pis'ma Zh. Eksp. Teor. Fiz. 44 (1986) 89 (Sov. Phys. JETP Lett. 44 (1986) 144); N. Dupuis et al., Phys. Rev. Lett. 70 (1993) 2613.
- [172] S. M. Anlage and U. Klein, J. Phys.: Condens. Matter, 12 (2000) L471.
- [173] H. Shimahara and D. Rainer, J. Phys. Soc. Jpn. 66 (1997) 3591.
- [174] H. Shimahara, Phys. Rev. B 50 (1994) 12760.
- [175] V. Jaccarino and M. Peter, Phys. Rev. Lett. 9 290 (1962).
- [176] H. W. Meul, et al., Phys. Rev. Lett. 53, 497 (1984).
- [177] L. Balicas, J. S. Brooks, K. Storr, S. Uji, M. Tokumoto, H. Tanaka, H. Kobayashi, A. Kobayashi, V. Barzykin, and L. P. Gor'kov preprint cond-m at 0103463, Phys. Rev. Lett. 87, 067002 (2001)
- [178] H. Frolich, Proc. R. Soc. Ser. A 223, 296 (1954).
- [179] G. G. Lerner, Density waves in solids (Frontiers in Physics, vol 89) (Addison-Wesley, 1994).
- [180] A. Ardavan, N. Harrison, P. G. Oddard et al., preprint, submitted to Science; N. Harrison, preprint cond-m at 01110278.
- [181] M. M. Honold, N. Harrison, M. V. Kartsovnik, H. Yaguchi, J. Singleton, C. H. Mielke, N. D. Kushch, M. Kumoo and P. Day, Phys. Rev. B 62, 7908 (2000)
- [182] See e.g. R. H. McKenzie, J. Merino, J. B. Marston and O. P. Sushkov, preprint cond-m at 0102142 (2001).

